UNIVERSITY OF CAMBRIDGE

Numerical Analysis Reports

Reversible Adaptive Regularization I: Perturbed Kepler Motion and Classical Atomic Trajectories

B. Leimkuhler

DAMTP 1997/NA8
May 1997

Department of Applied Mathematics and Theoretical Physics
Silver Street
Cambridge
England CB3 9EW

Reversible Adaptive Regularization I: Perturbed Kepler Motion and Classical Atomic Trajectories

Benedict Leimkuhler *

May 13, 1997

Abstract

Reversible and adaptive integration methods based on Kustaanheimo-Stiefel regularization and modified Sundman transformations are applied to simulate general perturbed Kepler motion and to compute classical trajectories of atomic systems (e.g. Rydberg atoms). The new family of reversible adaptive regularization (RAR) methods also conserve angular momentum and exhibit superior energy conservation and numerical stability in long time integrations. The schemes are appropriate for scattering, for astronomical calculations of escape time and long-term stability, and for classical and semiclassical studies of atomic dynamics with or without fields. The components of an algorithm for trajectory calculations are described. Numerical experiments illustrate the effectiveness of the reversible approach.

keywords: adaptive methods, time-reversible variable stepsizes, Hamiltonian systems, gravitational few-body problems, scattering, N-body problems, regularization, time-transformations, perturbed Kepler motion, semiclassical approximations, long term integration, Rydberg atoms.

*Dept. of Mathematics, 405 Snow Hall, University of Kansas, Lawrence, KS 66045, USA. leimkuhl@math.ukans.edu. Visiting DAMTP AY 1996-97. Research supported by NSF grant No. 9303223 and DAMTP.

1 Introduction

This paper describes the design of efficient time-reversible regularized adaptive methods for long term integration of Coulombic few-body problems. The stable computation of trajectories is important for astronomical applications [17, 22, 1] and in the classical and semi-classical studies of atomic systems, particularly atoms in highly excited ('Rydberg atom') states [12, 30, 7, 28, 23, 25, 13, 31]. Calculations of relevant stochastic quantities (average escape time, orbital dimension, etc.) may require long time integrations. Using traditional methods, very small timesteps or nonphysical corrective measures—such as rescaling of velocities—are sometimes needed to maintain roughly constant energy throughout a long simulation.

While preservation of symplectic structure is known to lead to improved conservation of energy in long term simulations [34, 15, 3], we show that, at least in two-body scattering, discrete conservation of the symmetry and time-reversal symmetry implies an orbital axial symmetry which again confers superior energy conservation. Although this result is restricted to the two-body case, our numerical experiments suggest that the property is potent enough to facilitate stable long term integration of perturbed Kepler motion and atomic few-body problems when a splitting technique is used to isolate the strong two-body contributions to the motion. Our method also conserves angular momentum.

Although some of the observations of this article would be applicable to other types of systems, we will focus on N-body problems with Hamiltonian

$$H = \sum_{i=1}^{N} \frac{|p_i|^2}{2m_i} - V(q)$$

Here $V(q)$ is a potential energy function which is assumed to decompose into Coulombic two-body interactions.

$$V(q) = \sum_{i=1}^{N-1} \sum_{j=i+1}^{N} \frac{\alpha_{ij}}{r_{ij}}$$

For gravitation, all of the terms α_{ij} are negative, whereas for atomic problems, both signs occur. To simplify the presentation, we will typically assume unit masses and that the constants α_{ij} are ± 1.

For atomic problems, the nuclei may often be assumed fixed in space to first approximation, resulting in a reduced Hamiltonian for the electron motion.

The two types of Coulombic problems are similar in that there are always some negative force coefficients α_{ij}. This makes possible arbitrarily close approaches of two bodies ("collisions") which are ruled out in other N-body systems such as molecular dynamics (due to Pauli repulsion). Gravitation and classical atomic dynamics differ in that three-body collisions, although rare in gravitation [35], are rarer still in atomic systems. For example, the only way to have a three-body collision in helium is along a zero-angular momentum orbit when the two electrons approach the nucleus from either side, and even with $l = 0$, this occurence appears to be exceptionally rare. This article focuses on the treatment of perturbed Kepler motion and atomic problems, i.e. problems without close three-body approaches. A companion article will consider extension of the reversible adaptive regularization method for gravitational N-body simulation.

Time-transformations alone can be used as smoothing transformations for two-body collisions [18, 19], however much better results are obtained when they are combined with various types of coordinate transformations (Kustaanheimo-Stiefel (KS) transformation, semi-parabolic coordinates, etc.). These have the effect of reducing the pure Kepler problem to a linear system. When the KS transformation is used to generate a timestepping method in the context of perturbations, the key problem turns out to be the efficient resolution of the time variable. We take up these issues in §4. One component of our overall method is a regularizing energy–conserving symplectic Kepler solver that is more efficient than a standard quadrature.

Even with regularization, time transformations per se are still very important for two reasons: (1) we find that despite the use of a regularizing transformation, the *sensitivity* of the Keplerian motion to distant perturbing forces increases substantially during a collision, and (2) they are needed for treating the still quite strong forces, such as electron-electron interactions, which are not regularized by the KS transformation. Our method therefore also includes the use of an outer modified Sundman transformation incorporating these effects. A third use for the Sundman transformation is to automatically reduce the stepsize during very large motions such as occur during ionization in an external field.

The glue that binds all these techniques together is the fully explicit Adaptive Verlet method of [18], which allows us to incorporate the Sundman transformation in such a way that the overall timestepping strategy preserves the time-reversal symmetry of the true flow. Although symplecticness is then sacrificed; our experiments (see also [19, 9]) show that this conservation is adequate to recover long-term behavior reminiscent of symplectic methods. While experiments in [2] with Lennard-Jones hard-walls suggested the possibility of instability in explicit variants of Adaptive Verlet, we do not observe any such problems in the current application provided the control is properly chosen, probably because the AV scheme is only being used to control timestep with respect to (relatively) soft forces, after the collisions have been ameliorated by regularization.

A recent article appearing in the astrophysics literature [9] describes a method for combining the KS transformation with time-reversible stepsize variation for treating perturbed Kepler motion. This study did not consider multiple-body problems and it uses the implicit stepsize variation technique of [19] instead of an explicit scheme such as that described here; for this reason, we believe that our method will prove to be substantially more efficient in highly collisional problems.

The layout of the paper is as follows. In §2, we discuss the energy error when a simple scattering problem is solved with various numerical methods, and point out that even the short term dynamics of a collisional problem benefit from a symplectic scheme. In §3, we demonstrate with a numerical experiment that time-reversible schemes applied to the time-transformed equations of motion also give excellent energy conservation, and we introduce the Adaptive Verlet method. §4 discusses regularizing transformations and the fast Kepler solver. §5 discusses and compares several methods for treating perturbed Kepler problems. §6 describes the treatment of atomic systems based on splitting, the fast Kepler solver, and Adaptive Verlet. §7 revisits a scattering study that recently appeared in the physical literature; by using the new reversible adaptive regularization method, finer structure is obtained in the regime of chaotic scattering. Appendices include (Appendix A) standard numerical methods, (Appendix B) description of the reversible adaptive regularization algorithm for both perturbed Kepler and atomic problems, and (Appendix C) the extension of the method needed to incorporate magnetic and electrical fields.

All of the numerical experiments of §5-§7 and Appendix C were performed using the code **SCAT**, a C-language program avaliable from the author for simulating perturbed Kepler motion and classical atomic trajectories.

2 Background: Symplectic Methods in Numerical Scattering

In this section, we discuss the behavior of various types of numerical integration methods when applied to a simple scattering problem, the Kepler problem with Hamiltonian in polar coordinates given by

$$H = \frac{1}{2}p^2 - \frac{1}{q} + \frac{l^2}{2q^2}, \tag{2.1}$$

where $l = p_\theta$ is the angular momentum. The observations of this section generally apply to other collisional problems, such as the Kepler problem solved in cartesian coordinates, or problems with purely repulsive potentials such as the Lennard-Jones molecular potential.

We integrate a fairly low energy open orbit ($l = .5$, $H = 0.3975$) with six numerical methods. All of these methods are given in Appendix A. None of these schemes is energy-conserving, so we expect the energy to fluctuate with time, especially in the vicinity of the closest approach to the fixed body.

The graphs of numerical energy are shown in Fig. 1. For all of the six methods, energy variation is mild until perihelion, where one observes a sudden rapid variation. Qualitatively, the picture does not depend much on the stepsize or other parameters. In the first three methods, the energy does not return to the pre-collision level, whereas for each of the last three methods, the energy exhibits a remarkable stability through the collision, generally returning to very near the pre-collision energy level. Methods which have this property prove to be very effective for long time-interval computations. The difference between the methods is that the first three are all nonsymplectic methods, while the last three are all symplectic, i.e., they preserve the wedge product of differentials at each timestep:

$$dq_{n+1} \wedge dp_{n+1} = dq_n \wedge dp_n.$$

The drift can be studied with the aid of the *modified equations* [39], a system of differential equations whose exact solution agrees with the discretization to some arbitrary prescribed order.

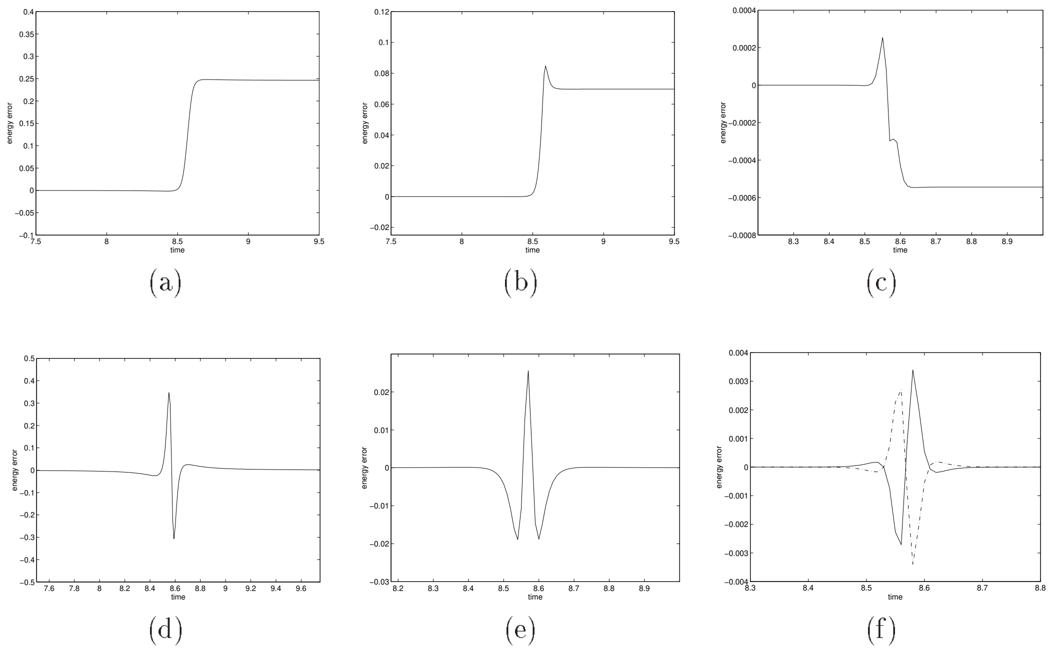

Figure 1: Energy Profiles During Two-Body Scattering: (a) Euler's Method, (b) Heun's Method, (c) 4th order Runge-Kutta, (d) symplectic Euler, (e) leapfrog/Verlet, (f) 3rd order Ruth method (-) and the 'adjoint' method (–). Stepsize for Euler's method $\Delta t = 0.001$; all others used $\Delta t = 0.01$.

Given an initial value problem of the form

$$\frac{d}{dt} z = f(z), \qquad z(0) = z_0,$$

where f is a C^∞ vector field. We compute numerical trajectories using a pth order numerical method

$$z_{n+1} = \Phi_{\Delta t}(z_n).$$

Here z_n is an approximation to $z(t_n)$, where $t_n = n\Delta t$.

The idea of the modified equations is to construct a flow which coincides with the numerical solution (to some arbitrary prescribed order). This can typically be done by matching terms in an asymptotic expansion in powers of Δt:

$$\tilde{f}_{\Delta t} = f + \Delta t f^{(1)} + \Delta t^2 f^{(2)} + \cdots$$

We compute the terms in the expansion recursively by demanding that the solution $\bar{z}$ of

$$\frac{d}{dt} \bar{z} = \tilde{f}_{\Delta t}(\bar{z}), \qquad \bar{z}(0) = z_n$$

agree with the numerical solution after one step to a given order in Δt.

The modified equations allow us to use continuous dynamical systems concepts to analyze near-to-the-identity discrete maps. An important property of the modified equations is summarized in the following "meta-theorem:" *the modified equations inherit integrals, symmetries, reversing symmetries and symplectic structure from the discretization*. Special cases of this result are proved in [34, 15, 11]). The special case for a symmetry or reversing symmetry does not appear to have been written down, but would follow by use of a similar argument to that contained in [11].

For a symplectic method, the meta-theorem implies the existence of a perturbed Hamiltonian expansion

$$\tilde{H}^{(k)}_{\Delta t} = H + \Delta t H^{(1)} + \ldots$$

whose exact solution agrees, to any prescribed order in Δt, with the numerical solution [34]. For example, in the case of the symplectic Euler method applied to (2.1), the first two terms of the perturbed Hamiltonian are

$$\tilde{H}^{(1)}_{\Delta t} = H - \frac{1}{2}\Delta t p\left(\frac{1}{q^2} - \frac{l^2}{q^3}\right).$$

More generally, we can compute the terms of the nearby Hamiltonian for a symplectic Runge-Kutta or partitioned Runge-Kutta method by appealing to the theory of trees [15, 34], in which case the precise form of the individual terms can be described ("elementary Hamiltonians"). Still more generally, such a series can be shown to exist for *any* symplectic map which is a smooth perturbation of the identity [24, 3].

Fixing any finite number of terms, it is straightforward to show that each finite higher order term (involving Δt^k, $k \geq 1$) of the modified equations includes a reciprocal power of q and hence vanishes as $q \to \infty$, but this is not quite the whole story, since the series expansion does not usually converge. Benettin and Giorgilli [3] recently carried out an asymptotic study of the perturbed Hamiltonian expansion to show that symplectic methods always have the property that the energy tends to within $O(\exp(-1/\Delta t))$ of the pre-collision energy following a scattering event. In the few-body problem, this strong conservation property (the existence of the perturbed Hamiltonian and its properties) apparently explains the superiority of symplectic methods compared to nonsymplectic methods. However, it is important to recognize that the bound in terms of $O(\exp(-1/\Delta t))$ is only valid in an asymptotic sense, for small stepsizes (for which the error is very small); at large stepsizes, the energy variation is complex and unpredictable.

Returning to the Figs.1d,e,f, we comment on the appearance of the graphs. For the symplectic Euler method it is easy to see that,

$$\tilde{H}^{(1)}(q,-p) + \tilde{H}^{(1)}(q,p) = 2H(q,p) + O(\Delta t^2), \tag{2.2}$$

hence

$$\tilde{H}^{(1)}(q,0) = H(q,0) + O(\Delta t^2),$$

and, using (2.2) together with $H(q,-p) = H(q,p)$, the Poisson bracket of H and $\tilde{H}^{(1)}$ satisfies[1]

$$\{H(q,p), \tilde{H}^{(1)}(q,p)\} \quad = \quad -\{H(q,p), 2H(q,p) - \tilde{H}^{(1)}(q,-p)\}$$

[1] The Poisson bracket $\{f,g\} := \nabla_q f \cdot \nabla_p g - \nabla_p f \cdot \nabla_q g_q$ of functions $f = f(q,p)$, $g = g(q,p)$ can be viewed as the time rate of change of a function f along a trajectory of the Hamiltonian system with Hamiltonian g.

$$= \quad -\{H(q,p), \tilde{H}^{(1)}(q,-p)\} + O(\Delta t^2).$$

Let $\Psi(t)$ represent the energy at time t obtained by integrating the modified equations forward in time from a point $(q,p) = (q_*, 0)$ at $t = 0$, then

$$\begin{aligned} \Psi(t) &= H(q_*, 0) + \int_0^t \dot{H} ds \\ &= H(q_*, 0) + \int_0^t \{H(q,p), \tilde{H}^{(1)}(q,p)\} ds + O(\Delta t^2). \end{aligned}$$

Integrating backward in time is equivalent (up to the change in the sign of p) to integrating forward in time using the Hamiltonian $\tilde{H}^{(1)}(q,-p)$, thus,

$$\begin{aligned} \Psi(-t) &= H(q_*, 0) + \int_0^t \{H(q,p), \tilde{H}^{(1)}(q,-p)\} ds + O(\Delta t^2), \\ &= H(q_*, 0) - \int_0^t \{H(q,p), \tilde{H}^{(1)}(q,p)\} ds + O(\Delta t^2). \end{aligned}$$

Finally,

$$\frac{\Psi(t) + \Psi(-t)}{2} = H(q_*, 0) + O(\Delta t^2),$$

which explains the antisymmetric appearance of the observed energy curve in Fig. 1d. Higher order symplectic methods would have a more complicated energy profile even in the leading term. An example is the third order Ruth method [32] whose energy is shown in Fig. 1f (the adjoint method is also shown).

A more popular symplectic method for N-body calculations is the leapfrog or Verlet integrator. This method also respects the time reversal symmetry typically present in physical systems:

$$\Phi_{\Delta t} \circ R = R \circ \Phi_{-\Delta t},$$

where

$$R\left(\begin{bmatrix} q \\ p \end{bmatrix}\right) = \begin{bmatrix} q \\ -p \end{bmatrix}.$$

This fact is a consequence of the fact that the adjoint method, $\Phi^*_{\Delta t} := \Phi^{-1}_{-\Delta t}$, coincides with the method itself: $\Phi^*_{\Delta t} = \Phi_{\Delta t}$. The energy profile for the leapfrog method is shown in Fig. 1e. Note that where the graph of the energy of the symplectic Euler method is roughly antisymmetric about the point of collision, the graph of the leapfrog scheme is symmetric about this point. This follows from the fact that the perturbed Hamiltonian of the leapfrog method is, like the original Hamiltonian, invariant under the involution $p \to -p$, hence an orbit crossing the symmetry plane (here the line $p = 0$) must be symmetric about that plane.

In the next section, we will see that the symmetry property of the energy graph in this application can be viewed as a consequence of just the preservation of symmetries of the differential equations.

3 Variable Stepsizes: A Reversible Method

It is natural to consider the use of a variable stepsize method for solving a problem such as scattering for which the solution is subject to sudden catastrophic events. Yet the results of using standard (nonconserving) variable stepsize methods are not much better than the results obtained for fixed stepsize methods. An example of a simple but popular variable stepsize method is the Runge-Kutta Fehlberg 4(5) embedded pair scheme, as implemented in MATLAB4.0. This method computes the new step by (1) applying a 4th order RK method, (2) computing a further 5th order approximation using the computed values of the vector field, then (3) adjusting the stepsize so that the difference between the two methods is less than a prescribed tolerance. A typical energy profile is shown in Fig. 2a. The additional dynamics induced by the stepsize selection strategy are rather complicated, so one cannot expect the energy profiles to scale in a simple way with the tolerance. Even if the method used is symplectic, a traditional stepsize variation method will destroy the conservative property of the method [6].

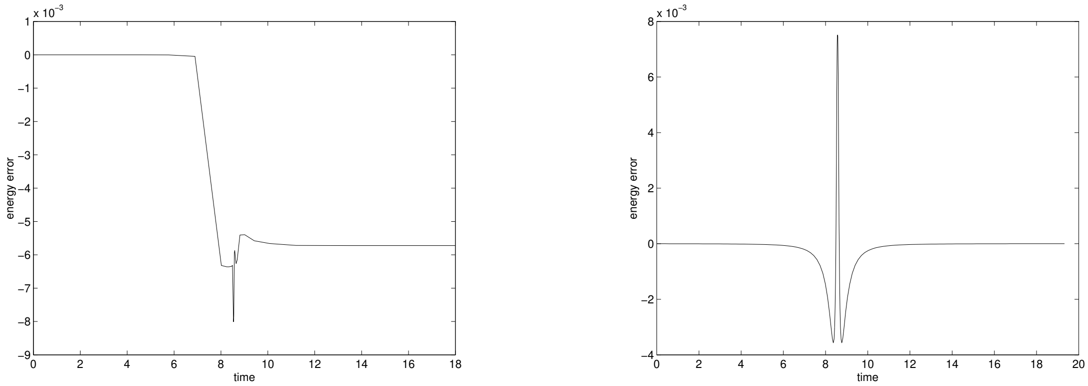

(a) (b)

Figure 2: Energy Profiles of Variable Stepsize Methods: (a) RKF 4(5), tolerance 0.001, (b) a reversible method based on implicit midpoint, fictive step $\Delta\tau = 0.2$.

A better way to incorporate timestep variation in a conservative system is to use an time-transformation which preserves structure.

3.1 Time-Transformations of Sundman and Poincaré.

A general Sundman transformation of time, introduces a new "artificial time" variable τ by

$$\frac{dt}{d\tau} = g(q,p),$$

where g is an arbitrary smooth, positive, scalar-valued function. The differential equations can then be written in terms of the independent variable τ as

$$\frac{d}{d\tau}q \quad = \quad g\nabla_p H,$$

$$\frac{d}{d\tau}p = -g\nabla_q H.$$

A solution of the scaled system is thus equivalent to that of the original system up to a reparameterization of time.

If the rescaled equations of motion are integrated with fixed stepsizes $\Delta\tau$ in artificial time, it is as if the timestep was being adjusted according to the size of the scaling function g:

$$\Delta t \approx g\Delta\tau.$$

For Hamiltonian systems, it may be more appealing to use a *Poincaré transformation* of the form

$$\tilde{H} = g(q,p)(H - H_0),$$

where H_0 is the energy of a particular desired orbit. The differential equations corresponding to $\tilde{H}$ can be written

$$\frac{d}{d\tau}q = g\nabla_p H + (H - H_0)\nabla_p g, \tag{3.3}$$

$$\frac{d}{d\tau}p = -g\nabla_q H - (H - H_0)\nabla_q g. \tag{3.4}$$

Note that along any particular orbit with energy $H = H_0$, the second term on the right hand side of the each of the differential equations will vanish and we are left with the Sundman transformed equations of motion. However, in the course of numerical integrations, there are typically some errors introduced in the energy, and the two approaches are then quite different.

The two types of time transformations provide different approaches to adaptive integration. If the discretization of the reparameterized equations preserves a geometric structure, then we can view the resulting method as a structure-preserving variable stepsize method. For example, when the Poincaré transformation is used, then a symplectic stepsize variation method can be obtained [29, 14]; e.g. a symplectic, second order method is obtained by solving (3.3)-(3.4) using the implicit generalized leapfrog discretization (Lobatto IIIA-B Partitioned Runge-Kutta method) [14].

If a Sundman time-transformation is positive and invariant under the involution $p \to -p$, then the rescaled equations of motion will possess the time-reversal symmetry, and use of an appropriate discretization scheme results in a time-reversible variable stepsize strategy [37, 19, 18].

We will illustrate the use of the time-reversible method with the simple scattering problem. We take

$$\frac{dt}{d\tau} = g := \frac{q^2}{1+q^2}.$$

This time transformation is carefully chosen so that (1) at a close approach ($q \approx 0$) a unit step in τ corresponds to a very small step in t (proportional to $|q|^2$), while (2) when q is large the steps in t corresponding to fixed steps in τ remain bounded. Applied to the polar Kepler problem, the time transformation leads to equations

$$\dot{q} = g(q)p,$$

$$\dot{p} = g(q)\left(-\frac{1}{q^2} + \frac{l^2}{q^3}\right).$$

These equations are no longer Hamiltonian, although the time-reversal symmetry is preserved. We solve the differential equations using the implicit midpoint method,

$$\begin{aligned} \bar{q} &= q_n + \tfrac{\Delta\tau}{2} g(\bar{q})\bar{p}, & \bar{q} &= (q_n + q_{n+1})/2, \\ \bar{p} &= p_n + \tfrac{\Delta\tau}{2} g(\bar{q})(-\tfrac{1}{\bar{q}^2} + \tfrac{l^2}{\bar{q}^3}), & \bar{p} &= (p_n + p_{n+1})/2, \end{aligned}$$

and also update the time variable using this method:

$$t_{n+1} = t_n + \Delta\tau g(\bar{q}).$$

The approach described is not symplectic. Yet its energy profile, shown in Fig. 2b, is similar to those of the symplectic schemes. This reflects a frequent observation in the literature: time-reversible integration schemes give excellent results in long term integrations. For a general discussion of symmetries and reversing symmetries in discretization see [27]. For a recent example comparing symplectic, reversible and traditional integration methods for a large dimensional nonlinear physical problem (a Heisenberg ferromagnetic system), see [8]. While we do not have a complete understanding of why the reversible methods perform very well, we can give a fairly detailed explanation in the case of the Kepler problem where axial symmetry of orbits is key.

3.2 Axial Symmetry in Scattering with Reversible Adaptive Methods

For the one degree of freedom Kepler problem in polar coordinates, it is easy to see why the energy rebounds to the pre-collisional level when a reversible adaptive method is used. Observe that the modified equations (any finite truncation of the modified equations) must also possess the reversing symmetry (by the meta-theorem stated in the last section). The orbit of the modified equations crosses the symmetry line $p = 0$, say at $q = q_*$. Integrating the equations forward in time from $(q_*, 0)$ or backwards in time from this point results in exactly the same trajectory up to the sign of p, hence also the energy is the same after integrating τ units either forward or backward in time, since H is an even function of p. This explains the symmetry observed in Fig. 2.

The argument does not immediately extend to the planar Kepler problem treated in the standard cartesian coordinates, since orbits do not penetrate the symmetry plane $p_1 = p_2 = 0$, but we show that an energy stability result can still be expected for the Kepler problem, provided both the time transformation and discretization preserve both the symmetry and time-reversal symmetry of the system.

After Sundman transformation, we have

$$\begin{aligned} \dot{q} &= g(q,p)p, & (3.5) \\ \dot{p} &= -g(q,p)q/|q|^3. & (3.6) \end{aligned}$$

The Kepler problem ($g = 1$ in (3.5)-(3.6)) possesses both a reversing symmetry $\mathcal{R}$: $t \to -t$, $p \to -p$, and symmetries of the form $\mathcal{S}$: $q \to Sq$, $p \to Sp$ for any orthogonal transformation S. (There is also an invariance under translation of time.) These symmetries are also preserved by the rescaled equations provided

$$
\begin{aligned}
g(q,p) &> 0, &&& (3.7)\\
g(q,-p) &= g(q,p), &&& (3.8)\\
g(Sq,Sp) &= g(q,p), && SS^T = I. & (3.9)
\end{aligned}
$$

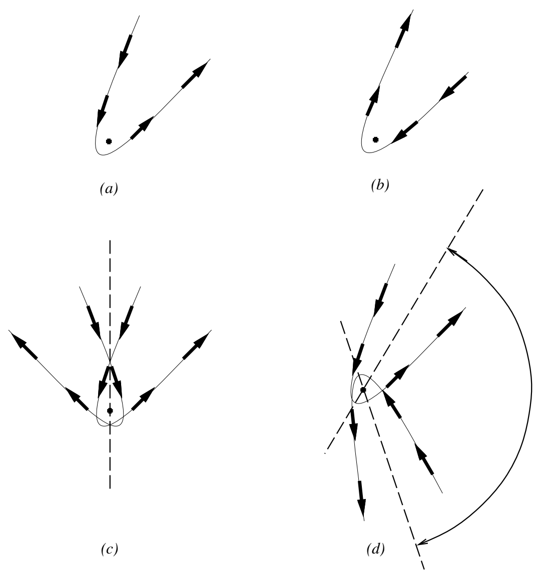

Figure 3: (a) A Kepler orbit, (b) its time-reversal, (c) a flip symmetry, (d) a rotational symmetry.

Not wishing to introduce an overly-grandiose term for the property, a Sundman transformation preserving (3.7)-(3.9) will be termed *appropriate* for the Kepler problem. In particular, any $g = g(|q|) > 0$ is an appropriate Sundman transformation. Similarly, we will call a discretization scheme appropriate if it respects the symmetry and reversing symmetry of a given system. Most discretization schemes preserve the linear symmetry of the Kepler problem, but relatively few preserve the reversing symmetry.

In terms of a given orbit $O = \{(t, q(t), p(t))|t \in \mathbb{R}\}$ (Fig. 3a), the time-reversal symmetry means that $\mathcal{R}O = \{(t, q(-t), -p(-t))|t \in \mathbb{R}\}$ is also an orbit (Fig. 3b). The symmetry means that $\mathcal{S}O = \{(t, Sq(t), Sp(t))|t \in \mathbb{R}\}$, where $SS^T = I$, is again an orbit. Note that the symmetry group includes both rotations and flips (Fig. 3c,d).

The orbits of the Kepler problem are *axially symmetric* implying that there is a particular flip symmetry which, when followed by a time-reversal (and possibly a time-translation), leaves the orbit invariant. The main result of this section is:

Theorem 1 *In the Kepler problem treated with an appropriate Sundman transformation and an appropriate discretization, every finite discrete orbit obtained with a sufficiently small timestep is axially symmetric.*

The key problem is to identify the axis of symmetry of the discrete orbit. We sketch the proof for the case of a positive energy orbit ($H_0 > 0$).

Perihelion is distinguished by the orthogonality condition $q \cdot p = 0$; the latter quantity changes sign through a collision. Now applying any appropriate Sundman transformation to the Kepler problem, one sees from (3.5)-(3.6) that

$$\frac{d}{dt} q \cdot p = g \frac{|p|^2}{2} + g H_0 > 0,$$

hence $q \cdot p$ is strictly monotone increasing along such an orbit. We can assume without loss of generality that the perihelion point ($q \cdot p = 0$) occurs at $t = 0$ (Fig. 4a).

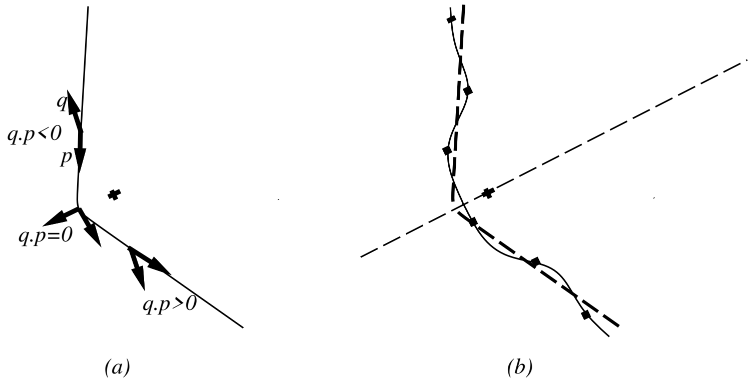

Figure 4: (a) $q \cdot p$ is monotone increasing, (b) An orbit (thick dashed), with a numerical solution (boxes), and a corresponding orbit of the modified equations (thin solid).

Consider a convergent appropriate discretization method and an orbit $O = \{(t, \bar{q}(t), \bar{p}(t)) | t \in \mathbb{R}\}$ of (a finite truncation of) the modified equations which starts from some point $(-T, q(-T), p(-T))$ of the true orbit. Set $\bar{\mu}(t) := \bar{q}(t) \cdot \bar{p}(t)$.

Since $q \cdot p$ is monotone in t, for sufficiently small timestep, $\bar{\mu}$ must be monotone on $[-T, T]$ (by convergence) and will have a zero, say at $t = t_*$ and $(q_*, p_*) = (\bar{q}(t_*), \bar{p}(t_*))$. With perhaps a shift in time, we can assume without loss of generality that $t_* = 0$.

q_* now defines our axis of symmetry. Let $\mathcal{S}_*$ be the flip symmetry defined by the ray through q_*. That is, we define $\mathcal{S}_*$ as the linear plane symmetry described by the orthogonal transformation $S_* = 2q_* q_*^T / |q_*|^2 - I$.

Applying the symmetry $\mathcal{S}_*$ to O, we get a new orbit. Applying the time-reversal symmetry $\mathcal{R}$ to O, we get yet another orbit. Clearly, $\mathcal{S}_* O$ includes the point $(0, q_*, -p_*)$, since $S_* q_* = q_*$, $S_* p_* = -p_*$. On the other hand, this point is also on the orbit $\mathcal{R}O$. By uniqueness of solutions to the initial value problem, the two orbits must be equivalent. Thus $\mathcal{S}_* O = \mathcal{R}O$, so $\mathcal{R}\mathcal{S}_* O = O$, and O is therefore axially symmetric. (Fig. 4b)

The case $H_0 = 0$ is essentially the same as above. For the bound case $H_0 < 0$, there are now two points with $q \cdot p = 0$ along the exact elliptical orbit (perihelion and aphelion); we identify either one of these to use in the proof above ($q \cdot p$ will still be monotone over each half of the ellipse containing a single extremal point).

□

The argument of Theorem 1 implies that the energy variation, too, is symmetric with respect to the perihelion approach. The theorem could easily be extended to include arbitrary central-force two-body problems in $\mathbb{R}^3$, for which the solutions are planar and posess the same symmetry features.

The argument of Theorem 1 breaks down, however, when three bodies interact at close range, and the energy no longer can be expected to return to very near its pre-collision value following such an event. Nonetheless, for the perturbed Kepler problem or for that matter the N-body problem, *most orbits appear Keplerian in the vicinity of close approach* due to the local dominance of the Coulombic force and the rarity of three-body collisions [35].

As we shall see in the following subsection, it is possible to formulate a powerful explicit scheme based on the reversible adaptive framework, and these methods can be quite powerful for N-body systems, especially when employed in combination with regularizing coordinate transformations.

3.3 The Adaptive Verlet Method

The Adaptive Verlet method of [18] provides a framework for discretizing the reparameterized equations in a reversible way. For a Hamiltonian system of the form $H(p,q) = T(p) + V(q)$, a related, fully explicit method consists of introducing a new variable ρ representing the reciprocal of the time-scaling factor and computed according to a symmetric recurrence relation. We then discretize by a three stage scheme [18, 2]:
I. Symplectic Euler half step.

$$\begin{aligned} q_{n+\frac{1}{2}} &= q_n + \frac{\Delta\tau}{2\rho_n}\nabla_p T(p_n) \\ p_{n+\frac{1}{2}} &= p_n - \frac{\Delta\tau}{2\rho_n}\nabla_q V(q_{n+\frac{1}{2}}) \end{aligned}$$

II. Update of the scaling factor ρ via the formula

$$\rho_n + \rho_{n+1} = \frac{2}{g(q_{n+\frac{1}{2}}, p_{n+\frac{1}{2}})} \tag{3.10}$$

III. Symplectic Euler adjoint half step.

$$\begin{aligned} q_{n+1} &= q_{n+\frac{1}{2}} + \frac{\Delta\tau}{2\rho_{n+1}}\nabla_p T(p_{n+1}) \\ p_{n+1} &= p_{n+\frac{1}{2}} - \frac{\Delta\tau}{2\rho_{n+1}}\nabla_q V(q_{n+\frac{1}{2}}) \end{aligned}$$

This method is a time-reversible generalization of Verlet (obtained when $g \equiv 1$). It also conserves the angular momentum of a system of particles. We sometimes use the method shifted by one half timestep, so that ρ is computed at the beginning, rather than in the middle, of each step.

Note that the Adaptive Verlet method is appropriate in the terminology of the last subsection.

The Adaptive Verlet method is similar to the "time-symmetrized" integrators discussed in [19, 9, 20], with a key difference: the latter methods are all based on an *implicit* formalism and require multiple force evaluations at a time step if the nonlinear equations are to be solved to roundoff and the method remain truly time-reversible.

The explicit scheme (3.10) had a tendency to develop oscillations or "wobble" in experiments of [2] on Lennard-Jones walls which resulted in decreased stability; however, we found that the explicit scheme works very well for stabilizing the relatively mild forces which remain after regularization of Coulombic collisions in the N-body problem, and there was no evidence of instability when the control was properly chosen. If wobble does lead to an instability, the semi-implicit variations given in [2] may offer improvement, without requiring multiple force evaluations at a timestep.

Heggie [16] suggested using time-transformations alone to regularize N-body problems; his idea can be combined with the reversible schemes. Heggie used

$$g = 1/U,$$

where U is the potential energy. For the Kepler problem, this means $g = |q|$. In our experience this gives some improvement over the unmodified Kepler problem but for stable integration in the presence of perturbations, a much stronger transformation of the form

$$g = |q|^2$$

is needed to carry out integration near the close approaches. The use of such an approach based solely on time transformation is not efficient for even moderately difficult trajectories in our experience (see §5).

In [33], the singularity of the Coulomb potential is removed by incorporating a small parameter, i.e $1/r \rightarrow 1/(r+\epsilon)$. This changes the structure of phase space in a fundamental way and eliminates many complicated orbits. While some justification is occasionally given for this type of "smoothing" in atomic problems on physical grounds (for multi-electron atoms, the perturbation can be viewed as induced by an excited electron in a close orbit around the nucleus, see citesm1), we prefer an approach based on the use of a combination of coordinate and time transformations to regularize the closest two-body approaches.

4 Fast Kepler Solver

A coordinate transformation $(q,p) \mapsto (Q,P)$ of the form

$$\begin{aligned} q &= \phi(Q), \\ \phi'(Q)^T p &= P, \end{aligned}$$

where ϕ is a diffeomorphism of $\mathbb{R}^N$, is called a 'cotangent lift transformation' [26]. Such a map is always necessarily symplectic (canonical), meaning that $\sum_i dq_i \wedge dp_i \equiv \sum_i dQ_i \wedge dP_i$. Under such a transformation, the Hamiltonian becomes

$$\bar{H}(Q,P) = H(\phi(Q), \phi'(Q)^{-T} P).$$

For the purposes of numerical integration, we can use a lift transformation as follows: (1) map initial conditions (q_0, p_0) to (Q_0, P_0) under the transformation, (2) integrate the differential equations for the transformed Hamiltonian $\bar{H}$ for some desired time t, and (3) map the solution back under the inverse transformation. Usually, we will have to perform step (2) using some (ideally symplectic) numerical integration procedure.

The traditional way of regularizing 2-body motion in N-body gravitational simulations is via the Kustaanheimo-Stiefel (KS) transformation. The idea is to introduce both coordinate and time transformations which reduce the 2-body problem to a linear system which is then easily solved. In N-body simulations, the coordinate transformations have the effect of stabilizing the numerical dynamics. This method, which generalizes the planar Levi-Civita regularization, can be implemented in a canonical framework. In $\mathbb{R}^4$ we introduce the coordinate transformation

$$\begin{bmatrix} q \\ 0 \end{bmatrix} = \phi(Q) = \mathscr{L}(Q)Q, \tag{4.11}$$

where Q is a 4-vector and $\mathscr{L}(Q)$ is the KS-matrix

$$\mathscr{L}(Q) = \begin{bmatrix} Q_1 & -Q_2 & -Q_3 & Q_4 \\ Q_2 & Q_1 & -Q_4 & -Q_3 \\ Q_3 & Q_4 & Q_1 & Q_2 \\ Q_4 & -Q_3 & Q_2 & -Q_1 \end{bmatrix} =: |Q|\mathscr{R}(Q),$$

with $\mathscr{R}$ an orthogonal matrix. The transformation has the property $|q| = |Q|^2$.

Note that

$$\phi'(Q) = 2\mathscr{L}(Q),$$

hence the canonical momenta P to Q are related to p directly by

$$\phi'^T \begin{bmatrix} p \\ 0 \end{bmatrix} = P \Rightarrow \begin{bmatrix} p \\ 0 \end{bmatrix} = \frac{1}{2|Q|}\mathscr{R}P. \tag{4.12}$$

The KS transformation introduces an S^1 symmetry through the following quadratic constraint on Q, P:

$$Q_4P_1 - Q_3P_2 + Q_2P_3 - Q_1P_4 = 0. \tag{4.13}$$

To put this another way, ϕ can be viewed as a map from $\mathbb{R}^4 \setminus S^1$ to $\mathbb{R}^3$. With this interpretation, the inverse map is well-defined and easily computable [21].

The Hamiltonian in the new variables is:

$$H = \frac{1}{8}\frac{|P|^2}{|Q|^2} - \frac{1}{|Q|^2}.$$

After a Poincare-type time transformation, we get a linear Hamiltonian system:

$$\tilde{H} = |Q|^2(H - H_0) = \frac{1}{8}|P|^2 - 1 - H_0|Q|^2.$$

It is important to insure that the initial values for Q and P are chosen so as to satisfy the constraint (4.13) but this equation then becomes an integral invariant of the transformed system (so it is satisfied automatically by the true flow).

The Poincaré transformation introduces a nonlinear scaling of time, i.e. the equations of motion are

$$\frac{d}{ds}Q = \frac{1}{4}P, \tag{4.14}$$

$$\frac{d}{ds}P = 2H_0Q, \tag{4.15}$$

$$\frac{dt}{ds} = |Q|^2.$$

Resolving the motion thus requires propogation of Q, P as the flow of a simple linear system, coupled to the scalar differential equation

$$\frac{ds}{dt} = |Q(s)|^{-2}.$$

If the solution is needed at a fixed time T, the resolution of the corresponding fictive time $S(T)$ is nontrivial, requiring the computation and inversion of the antiderivative function for $|Q|^2$. To perform this calculation, we write

$$F(S) := T - \int_0^S |Q(s)|^2 ds, \tag{4.16}$$

and apply scalar Newton iteration:

$$\begin{aligned} S^{(m+1)} &= S^{(m)} - \frac{F(S^{(m)})}{F'(S^{(m)})}. \\ &= S^{(m)} + \frac{F(S^{(m)})}{|Q(S^{(m)})|^2}. \end{aligned}$$

Since Q is determined by solving linear differential equations, the formulas can be greatly simplified, however this calculation introduces some overhead in the form of transcendental functions which must be reevaluated several times until convergence.

Since our method relies on very frequent computations of two-body problems, including resolution of the inverse time transformation, it becomes an expensive component of the algorithm. We have found that an alternative approach using the implicit midpoint discretization to solve the KS-transformed equations together with the equation of time is reliable and substantially cheaper than using the exact quadrature. Specifically, we solve

$$Q_{n+1} = Q_n + \frac{\Delta s}{4}P_{n+1/2}, \tag{4.17}$$

$$P_{n+1} = P_n + 2\Delta s H_0 Q_{n+1/2}, \tag{4.18}$$

$$\Delta t = \Delta s|Q^{n+1/2}|^2, \tag{4.19}$$

$$Q_{n+1/2} = \frac{Q_n + Q_{n+1}}{2},$$

$$P_{n+1/2} = \frac{P_n + P_{n+1}}{2}.$$

To solve this system, we write

$$Q_{n+1/2} = Q_n + \frac{\Delta s}{8}\left(P_n + \Delta s H_0 Q_{n+1/2}\right),$$

which gives an equation solvable for $Q_{n+1/2}$:

$$Q_{n+1/2} = (1 - \frac{\Delta s^2}{8} H_0)^{-1}(Q_n + \frac{\Delta s}{8} P_n).$$

Hence, after computing the squared two-norm and substituting into the equation of the timestep (4.19), we arrive at

$$F(\Delta s) := (1 - \frac{\Delta s^2}{8} H_0)^2 \Delta t - \Delta s \left(|Q_n|^2 + \frac{\Delta s}{4} Q_n \cdot P_n + \frac{\Delta s^2}{64}|P_n|^2\right) = 0. \qquad (4.20)$$

The equations thus reduce to a 4th degree polynomial equation for Δs, and no transcendental functions need to be evaluated. Although this quartic equation could be solved in radicals, it is much more economical to use a Newton iteration to resolve the time variable. As a stopping criterion for the Newton iteration, we used

$$\delta := |F/(\Delta s F')|, \qquad \delta/RTOL + |F|/ATOL < 1,$$

where, on a Pentium PC using double precision, $RTOL = 10^{-8}$, $ATOL = 10^{-11}$ worked well. Occasionally, we encountered difficulty with Newton convergence during very close approaches and suggest that a more robust modified Newton iteration [5] should be used in software.

The Kepler solution (and the resolution of the time variable) represented a substantial component of overall cpu time in our experiments. In typical runs, the fast Kepler solver reduced the overall CPU time for the code by a factor of more than 1.5.

The implicit midpoint method is symplectic and preserves all quadratic first integrals, such as the energy in transformed variables and the special constraint (4.13).[2] Except at extraordinarily close approaches to the fixed body (see §7 and Appendix C), we were unable to observe any substantive differences between algorithms based on exact quadrature and the fast Kepler solver in experiments, other than a substantial gap in performance. During very close approaches (within, say, 10^{-7}) the exact Kepler quadrature should probably be used for improved robustness.

5 Perturbed Kepler Motion

In this section, we will use the KS transformation to treat perturbed Keplerian motion, while taking advantage of the superior conservation properties of reversible adaptive integrators.

[2] Observe that the simultaneous conservation of energy and symplectic structure is only an apparent contradiction of the famous theorem of Ge and Marsden [10], since the conditions of that theorem specifically exclude integrable cases.

Consider the case of a perturbed two-body problem with Hamiltonian

$$H = \frac{1}{2}|p|^2 - \frac{1}{|q|} + \hat{H}(p, q).$$

Here we assume that $\hat{H}$ is a small perturbation.

One approach is to split H into the Kepler part and the perturbation, solving first the one with the KS transformation and the other with some symplectic integrator. That is, we set $\bar{H} = \frac{1}{2}|p|^2 - \frac{1}{|q|}$, and use the Strang splitting:

$$\exp \Delta t H = \exp \frac{1}{2}\Delta t \bar{H} \circ \exp \Delta t \hat{H} \circ \exp \frac{1}{2}\Delta t \bar{H} + O(\Delta t^2),$$

where $\exp tH$ is simply notation for the time t flow map of of the Hamiltonian H. We then solve $\bar{H}$ by introducing new variables Q, P and integrating the reparameterized system

$$\tilde{H} = |Q|^2(\bar{H} - \bar{H}_0). \tag{5.21}$$

In standard practice [1], non-symplectic, non-reversible methods would be used to integrate (5.21). In general it is found necessary to employ some sort of variable stepsize procedure in addition to the use of regularization.

We also found it necessary to incorporate a variable stepsize, but we do so in a time-reversible way, using an outer Sundman transformation together with the Adaptive Verlet method to perform our integration. For reasons discussed in the next section, we use a Sundman transformation of the form

$$g = \frac{1}{1 + |q|^{-1.5}}.$$

We will refer to this general approach as the reversible adaptive regularization or RAR method. For convenience, the algorithm is written out in detail in Appendix B.

As a first experiment, we solved the perturbed Kepler problem with Hamiltonian

$$H = \frac{1}{2}|p|^2 - \frac{1}{|q|} - \frac{1}{|q - q_1|},$$

viewed as describing a moving body around a fixed body located at the origin, in the presence of another fixed distant body (at q_1).

Placing the disturbing body at $q_1 = (0, 0, 5)$ we integrated what would be a moderately high eccentricity orbit for the unperturbed system using initial conditions $q(0) = (1.0, 0.0001, 0.0)$, $p(0) = (-1.0, 0.0, 0.0)$.

Graphs of the xy and xz projections of the trajectory are shown in Fig 5 for an integration on $[0, 1000]$. The full orbit appears to be quasiperiodic and is built up as follows in the xz projection: first a sequence of Kepler orbits is constructed on the right half of the nucleus, then the process is repeated on the left half. In each such basic cycle, the successive orbits vary from moderately eccentric to nearly circular (which marks the transition to the other side of the diagram). There is also a small oscillating precession visible in the xy plane projection. A graph of the energy error vs. time is shown if Fig. 6. Note that the energy is highly stable and that there

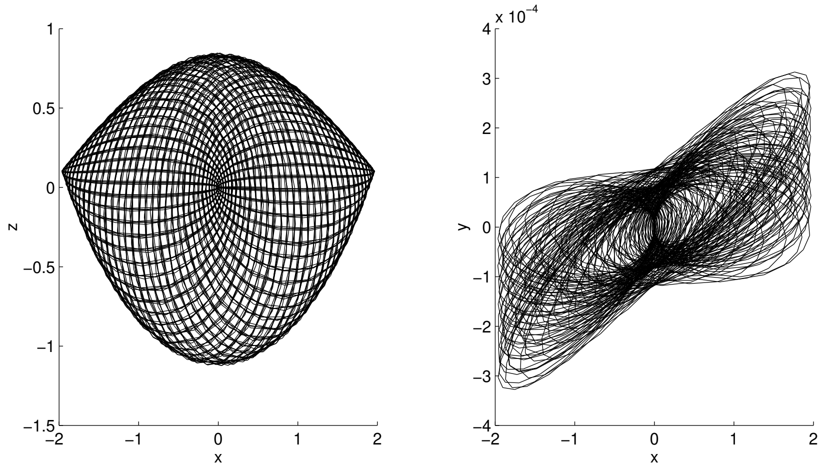

Figure 5: Views of the orbit: the disturbed Kepler problem.

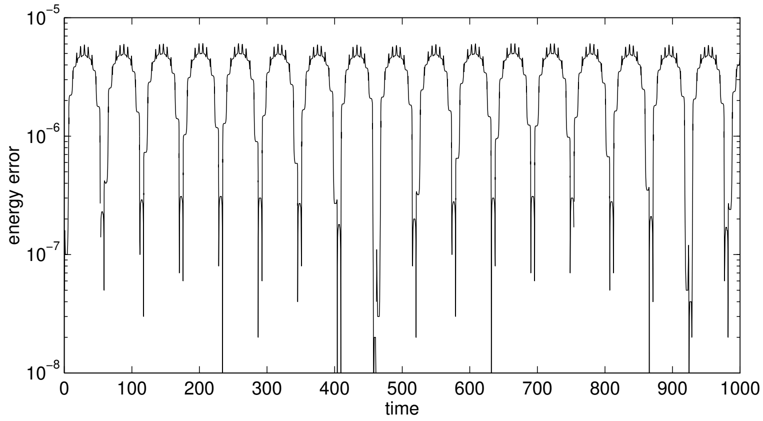

Figure 6: Energy errors for $\Delta\tau = 0.01$.

are no large spikes despite rather close approaches to the origin (within about 0.001). The quasiperiodic character of the motion is well resolved and there is no apparent systematic drift of energy.

The solution of the Kepler problems in the RAR scheme requires the accurate recovery of the time variable (via a quadrature) and inversion of the time transformation at each step if the step is to remain symplectic, and the overall method reversible. In an effort to avoid this cost, we tried methods which reverse the order of time and coordinate transformations, i.e. first perform a Poincaré transformation

$$\tilde{H} = |q|(\bar{H} + \hat{H} - H_0) \tag{5.22}$$

We can then split the Hamiltonian into Kepler part and perturbation:

$$\tilde{H} = \tilde{H}^{(1)} + \tilde{H}^{(2)}, \qquad \tilde{H}^{(1)} = |q|(\bar{H} - H_0), \qquad \tilde{H}^{(2)} = |q|\hat{H}. \tag{5.23}$$

The individual terms are then integrable successively: $H^{(1)}$ by introducing the KS coordinate transformation, and $H^{(2)}$ either by exact integration or by an appropriate numerical scheme. The key point is that both parts of the Hamiltonian are integrated in the same fictive time variable, so they are automatically synchronized and there is no need to invert the time transformation; the computation is thus completely explicit.

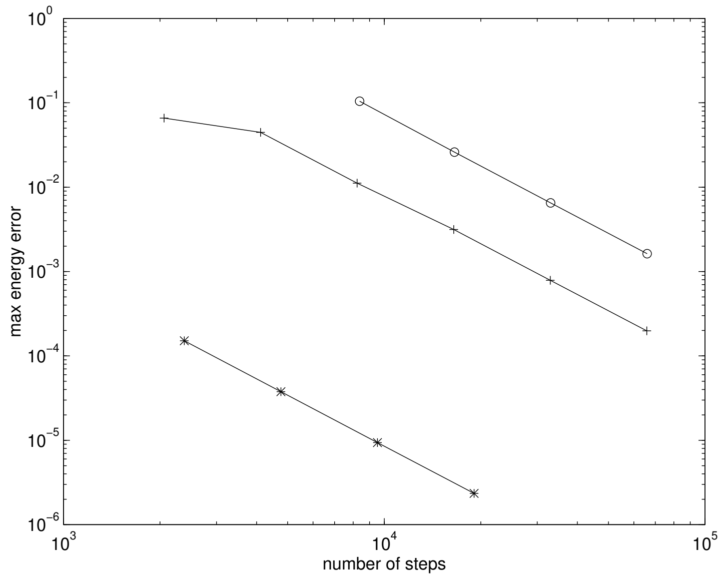

Figure 7: Comparison of work to energy for three methods: (1) '-o-' adaptive Verlet (no regularization), (2) '-+-' time-transformation followed by splitting, (3) '-*-' the RAR method.

However, this method did not compare favorably with the RAR method. When we integrated the disturbed Kepler problem, we still observed the noticeable spikes in energy present in fixed stepsize and unregularized variable stepsize simulations, although these were somewhat milder than before. The additional use of a Sundman transformation had little effect. The problem appears to be due to the fact that the value H_0 is the total energy of the system, not the energy of just the Kepler part in the vicinity of the close approach. During the close approach, this perturbation is significant and results in qualitatively incorrect dynamics.

Given that the RAR method can essentially stabilize the energy with respect to collisions, we see little advantage in using the alternative scheme.

We place the different schemes mentioned so far into perspective by constructing a work-energy diagram (Fig. 7) which compares the efficiencies of (1) the adaptive verlet (unregularized) method with $g = (1 + |q|^{-2})^{-1}$, (2) the modified scheme based on time transformation followed by splitting (5.23), (3) the RAR method with $g = (1+|q|^{-1.5})^{-1}$. Each point in the diagram represents one complete approximate trajectory on $[0, 100]$, requiring the indicated number of timesteps and producing the indicated maximum energy error. While the cost of a timestep is not the same for each of the methods, the additional work to perform coordinate transformations and to solve the scalar quartic polynomials required by the fast Kepler solver is easily justified by the huge reduction in numbers of timesteps needed for given accuracy.

The remarkable peformance improvement obtainable with the use of the regularizing transformation makes the procedure indispensable for perturbed Kepler motion. The combination of this procedure with reversible adaptive methods enables the efficient simulation of long time scale phenomena with little degradation of quasiperiodic structure. As we will see in the next sections and in Appendix C (electrical and magnetic fields), these benefits carry over to N-body problems of atomic type and for integrating chaotic trajectories.

6 Atomic Dynamics

Atomic dynamics can be handled using a generalization of the RAR method. This is possible because each electron generally participates in only two types of encounters: (1) collisions with the nucleus, and (2) interactions with the other electrons (or other pertubative forces). In this section, we outline an RAR-based algorithm for treating arbitrary atoms.

The algorithm is summarized for the convenience of the reader in Appendix B. The extensions to the algorithm needed for handling electrical and magnetic fields can be found in Appendix C.

The Hamiltonian for the atomic problem is, in standard atomic units and in the absence of fields,

$$H = \sum_{i=1}^{N} \frac{|p_i|^2}{2} - \sum_{i=1}^{N} \frac{k}{|q_i|} + \sum_{i=1}^{N-1} \sum_{j=i+1}^{N} \frac{1}{|q_i - q_j|}$$

where k is the charge on the nucleus. This Hamiltonian splits into $N+1$ parts:

$$\begin{aligned} H^{(i)} &= \frac{|p_i|^2}{2} - \frac{k}{|q_i|}, \qquad\qquad i = 1, \ldots, N, \\ V_{\mathrm{e-e}} &= \sum_{i=1}^{N-1} \sum_{j=i+1}^{N} \frac{1}{|q_i - q_j|} \end{aligned}$$

Each of the Kepler Hamiltonians can be integrated using the fast Kepler solver of §4, while the electron interaction term $V_{\mathrm{e-e}}$ is exactly integrable since it depends only on q.

The last component is the incorporation of a reversible stepsize variation procedure. The actual timestep needs to be decreased according to the difficulty of the Kepler problems (i.e. when $|q_i|$ becomes small), since these become more sensitive to the perturbing forces during close approach. A second problem has to do with electron-electron interactions which can occasionally lead to very strong forces, especially if one electron has recently undergone a strong acceleration via the Coulombic potential. Both of these difficulties are remedied by the use of an outer time transformation of the Sundman type.

6.1 A Sundman Transformation for Atomic Systems

The design of this time transformation is somewhat tricky. We considered various controls based on the two position dependent indicators (1) $r_{\text{en}} = \min_i |q_i|$, and (2) $r_{\text{ee}} = \min_{i \neq j} |q_i - q_j|$, of the form

$$g(q) = \frac{1}{r_{\text{en}}^{-a} + r_{\text{ee}}^{-b} + 1}. \tag{6.24}$$

Actually, a variety of different control strategies were explored, but others generally were less reliable; the suggested control proved to be remarkably robust when applied to a wide range of problems. There are good reasons for the choice of each term in (6.24), and the optimal powers a and b can be justified on the grounds of model problems and numerical experiments.

6.1.1 Electron-electron interaction.

The electron-electron interactions are not treated with any regularization other than the time transformation itself. We can gain insight into this term by considering the purely repulsive one degree of freedom problem with Hamiltonian

$$H = \frac{1}{2}p^2 + \frac{1}{q}, \qquad q > 0. \tag{6.25}$$

The idea is that a good time transformation for solving this special problem (in combination with a leapfrog-type splitting into kinetic and potential terms) should suggest a good time transformation for solving the general problem in regimes where the Keplerian part is mild.

The question is: what stepsize will control the energy drift during close approach? The answer is obtained by looking at the first two terms of the nearby Hamiltonian for the leapfrog method:

$$\tilde{H} = \frac{1}{2}(1 - \frac{1}{3}\Delta t^2 q^{-3})p^2 + q^{-1} + \frac{1}{12}\Delta t^2 q^{-4}.$$

As we have seen in §2, the energy error for leapfrog is worst near $q = q_*$ (closest approach, see Fig. 1c), at which point $p = 0$ in this problem and the error is

$$|\Delta H| \approx \frac{1}{12}\Delta t^2 q_*^{-4}$$

This suggests that the timestep control must be at least as strong as $\Delta t \sim q^2$ in the vicinity of the approach, if the energy error is to remain bounded (at least in the $O(\Delta t^2)$ term of the energy expansion).

To put this another way, by using $\Delta t = q^2 \Delta\tau$, we expect energy variation to be second order in $\Delta\tau$ with a coefficient independent of separation.

To test the design of the term based on the electron-electron potential, we used the orbit beginning from the initial conditions $q_1 = (1, 0, 0)$, $q_2 = (-1, 0, 0)$, and $p_1 = p_2 = (0, 1, 0)$. The two electrons follow symmetric orbits in the left and right

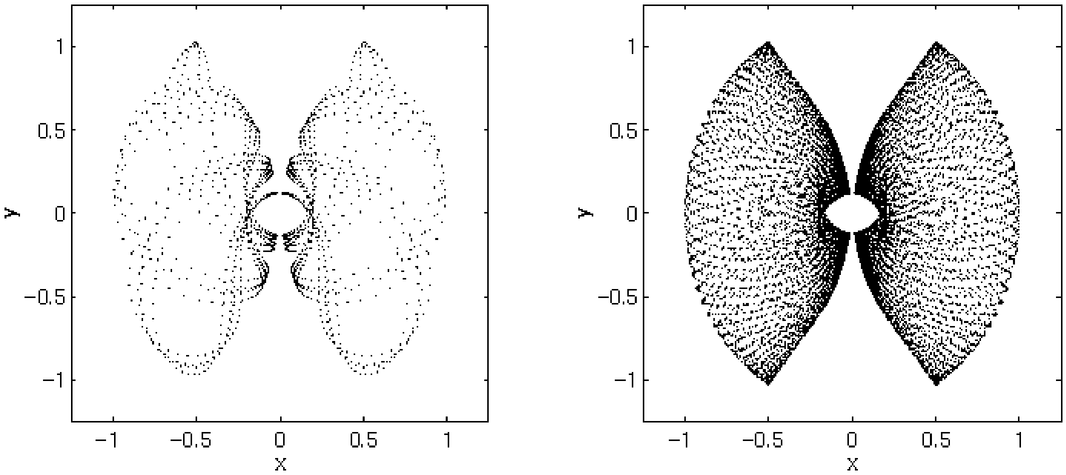

Figure 8: The first test orbit for Helium, near a Langmuir orbit, for which the timestep selection is dominated by electron-electron interactions. Left, to T=30; right, to T=300.

half-planes consisting of long smooth motions punctuated by varying strength e-e type collisions near the y-axis; the motion is shown in Fig. 8. This orbit is related to the Langmuir periodic orbit [36].

Fixing $a = 1.5$, we computed several trajectories on $[0, 30]$ for different values of b ($b = 0.0, 1.0, 1.5, 2.0, 2.5$) and of the stepsize; the resulting work-energy diagrams for each value of b are shown in Fig. 9. Clearly, there is a substantial gain in efficiency from involving $r_{\rm ee}$ in the control, and the optimal value is around $b = 2$. The resulting energy error and stepsize graphs are shown in Fig. 10.

6.1.2 Electron-nucleus interaction.

We can gain insight into the choice of the electron-nucleus interaction by considering the stability of the Kepler problem to perturbations. The equations of planar Kepler motion are

$$\begin{aligned} \dot{q} &= p, \\ \dot{p} &= -\frac{q}{|q|^3}. \end{aligned}$$

The variational equations describe the change over time in a perturbation evolved along a given trajectory by

$$\frac{d}{dt}\begin{bmatrix} \delta q \\ \delta p \end{bmatrix} = \begin{bmatrix} 0 & 1 \\ -\frac{1}{|q|^3} I + 3\frac{qq^T}{|q|^5} & 0 \end{bmatrix} \begin{bmatrix} \delta q \\ \delta p \end{bmatrix} =: A(t) \begin{bmatrix} \delta q \\ \delta p \end{bmatrix}.$$

In a single timestep, (q, p) doesn't change too much. Fix a point t_0. The eigenvectors and eigenvalues of $A = A(t_0)$ are

$$\xi_1 = \begin{bmatrix} q(t_0) \\ q(t_0) \end{bmatrix}, \qquad \lambda_{1,2} = \pm i |q(t_0)|^{-3/2},$$

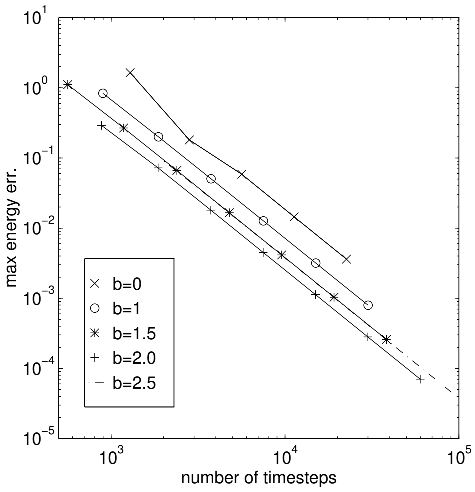

Figure 9: Work-energy diagrams comparing different values of b.

$$\xi_2 = \begin{bmatrix} q^{\perp}(t_0) \\ q^{\perp}(t_0) \end{bmatrix}, \qquad \lambda_{3,4} = \pm\sqrt{2}|q(t_0)|^{-3/2},$$

where $q^{\perp}$ is the orthogonal complement to q. The potentially large positive eigenvalue is capable of causing instability if excited by the numerical process. Let $\hat{\Phi}$ represent the propagator in one step. We have

$$\hat{\Phi} \approx \exp A(t_0)\Delta t,$$

with a principle unstable eigenvalue of

$$\gamma := \exp \sqrt{2}|q(t_0)|^{-3/2}\Delta t,$$

To control the potential for instability, it is thus necessary to limit the stepsize with

$$\Delta t \sim |\bar{q}|^{3/2}\Delta\tau$$

during the close approaches. In this way, the growth factor γ is independent of q and limited to

$$\gamma \sim 1 + O(\Delta\tau).$$

To test the design of the term based on the electron-nucleus potential, we used the orbit shown in Fig. 11. Here the first electron is started in an inner orbit, with $q_1 = (0.2, 0, 0)$, $p_1 = (0, 1, 0)$, while the second electron begins with $q_1 = (1, 0, 0)$, $q_2 = (0, 1, 0)$. The motion of the inner electron is strongly perturbed by the outer body, and the result is an essentially ergodic motion within a bounded region. The electron makes many very close approaches to the nucleus which would, if not resolved using the regularizing transformation, be essentially impossible to integrate numerically. Note in particular the appearance of Keplerian orbits during very close approach.

We conducted a sequence of experiments, fixing $b = 2.0$ and varying a. In this case, it proved impossible to integrate with values of $a < 1.5$ (the step scaling factor

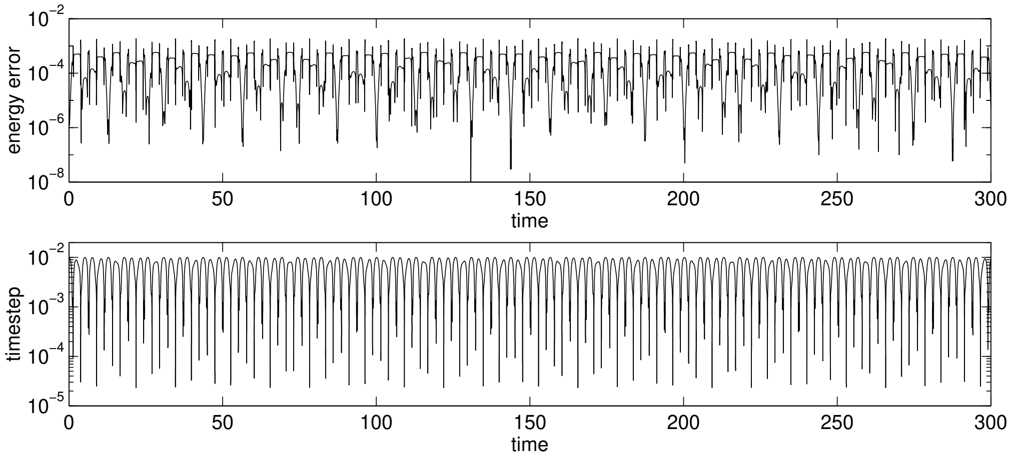

Figure 10: The energy errors and timestep variation observed for $b = 2$, $\Delta t_0 = 0.01$.

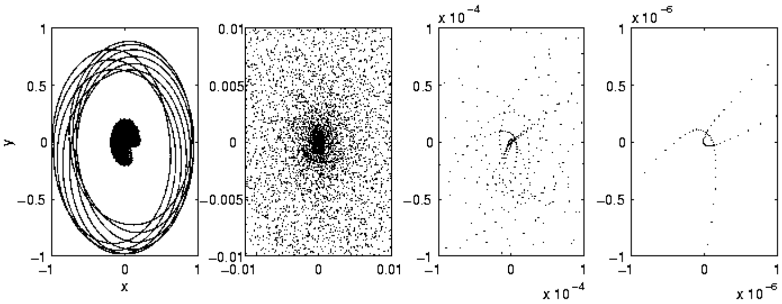

Figure 11: The second test orbit for Helium. Here the timestep is dominated by close approaches to the nucleus by the inner electron.

ρ tended to infinity, indicating instability of the integration process); this agrees with the observations made for the Kepler problem. For $a = 1.5$, on the other hand, the integration was very robust, and integration could be carried out for larger values of a, as well. We compare $a = 1.5$ and $a = 1.75$ in Fig. 12, showing the superiority of the lower value of a. For higher values of a, the results were substantially worse. With $a = 1.5$, the variations in timestep and the corresponding well-behaved energy error are shown in Fig. 13.

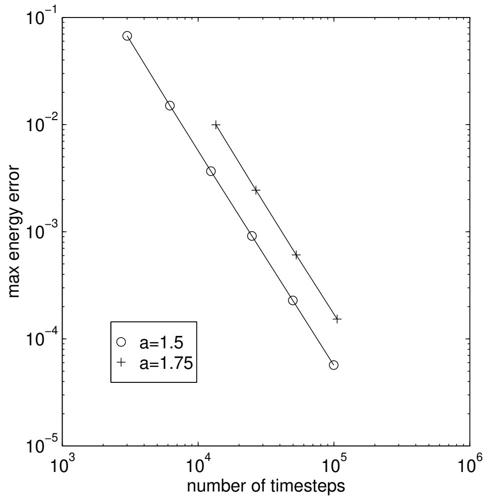

Figure 12: Work-energy diagrams comparing two different values of a; the computation was imposssible to carry out for smaller values of a due to instability.

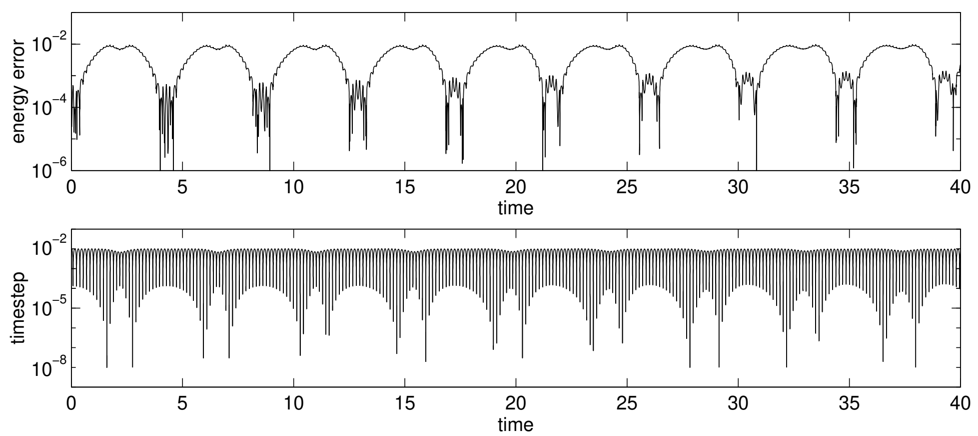

Figure 13: The energy errors and timestep variation observed for $a = 1.5$, $\Delta t_0 = 0.01$.

7 Application: He^+ Scattering

An article appearing in the physical literature [12] investigated the classical planar scattering of an electron from He^+. Using symbolic dynamics to organize the trajectories, they investigated escape rates and chaotic intermixing. Instead of using KS transformation, as here, the authors describe an ad hoc integration method which: (1) does not integrate the close approach (trajectories are tracked only to within about 10^{-5} of the nucleus) and (2) uses a standard variable step Runge-Kutta method.

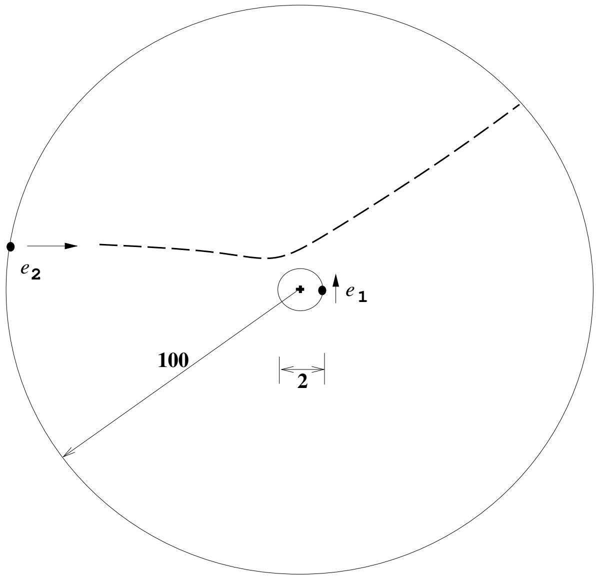

Figure 14: Scattering of He^+.

Our experiments are not precisely identical to those of [12] but are essentially equivalent. We used the same energies for each particle, and similar initial orbits. The only difference was in the exact configuration of the distant electron at time $t = 0$. In our experiment, the far electron is fired from a point on the circle of radius $R = 100$: $q_2(0) = (-\sqrt{R^2 - \beta^2}, \beta)$ with $p_2 = (.65, 0)$, with the inner electron started from initial data $q_1(0) = (0.833, 0)$, $p_1(0) = (0, 1.55)$. The situation is diagrammed in Fig. 14. In [12], the parameter β is obtained by simulating the motion of an electron in charge one Coulombic field up to the circle of radius R from an unspecified distant point; this also results in a very slight change in p_2; the difference in initial data is qualitatively inconsequential, effectively summarized by a slight shift in β. The computation is stopped following collision after one of the electrons reaches the circle of radius R, at which point the total collision time T_c is recorded.

We first performed a series of 1000 computations with $\Delta\tau = 0.01$, graphing T_c as a function of the scattering parameter $\beta \in [1.5, 2.5]$, Scattering diagrams for $\beta = 1.5..2.3$ in increments of 0.1 are shown in Fig. 15; the chaotic nature of some of the orbits becomes visible in close-ups of the collisional region (Fig. 16). Intervals in β of smoothly varying T_c are intermixed with chaotic regimes (Fig. 17). Large collision times are associated to long bounded excursions by one or the other electron (Fig.

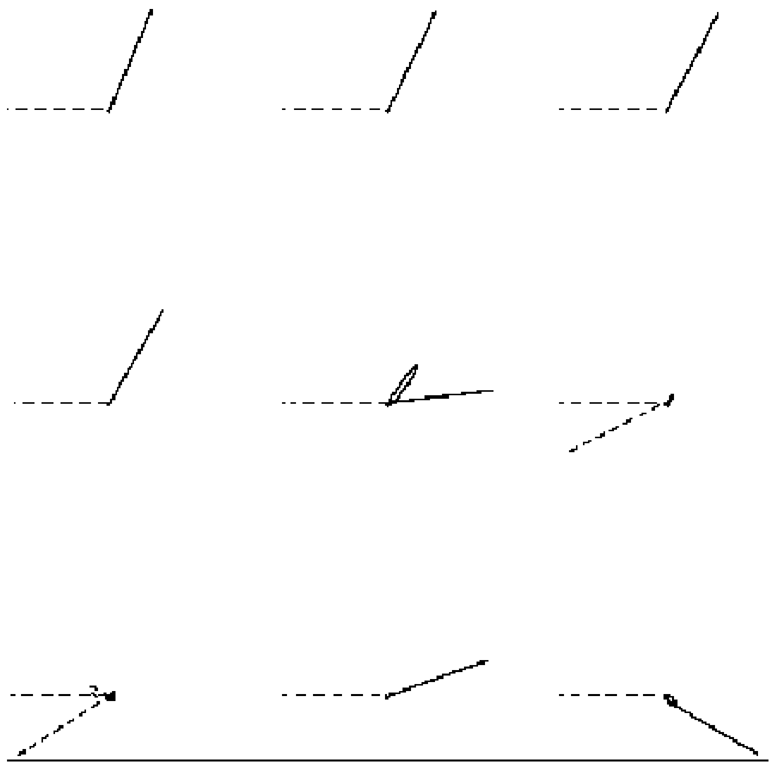

Figure 15: Scattering diagrams in the region $[-100, 100] \times [-100, 100]$ for β from 1.5 to 2.3, (β increases from left to right in each row). Initially distant electron (dashed); inner electron (solid)

18a). During such an excursion, the inner electron path is a series of short-period precessing elliptical orbits (slowly perturbed Kepler motion), often highly eccentric (Fig. 18b). The energy error increases markedly at the instant when the scattering electron arrives near the unit circle. This rise in energy is not unexpected since the trajectory becomes markedly more difficult to integrate at this instant. Fig. 19 shows the energy error and stepsize for the trajectory with $\beta = 2.1$. A reduced fictive timestep $\Delta\tau$ in the smooth regime correctly reduces the error by the square of the reduction factor (second order integration); however, this does not automatically hold in the chaotic regime, since a small change in the timestep may lead to a drastic change in the solution behavior (and potentially worse energy error).

The authors of [12] relied on the topological features of orbits computed in the chaotic regimes to calculate "escape rates from the chaotic repellers." The numerical problem becomes more difficult in the chaotic regime, where many close approaches increase the sensitivity of the solution to small perturbations; nonetheless, the reversible adaptive regularization is generally able to produce reasonable trajectories, with maximum energy error reasonably controlled for most trajectories in both the smooth or chaotic intervals (Fig. 22). Focusing on the subinterval $[1.8, 2.0]$, we observed that reduction of the stepsize did lead to apparent convergence of T_c in the

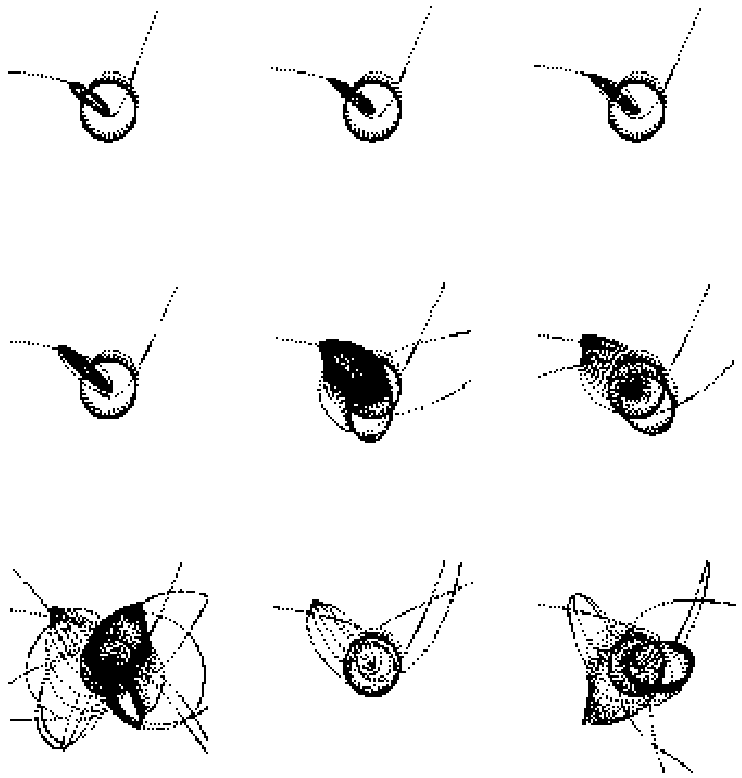

Figure 16: Collision region $(x, y) \in [-3, 3] \times [-3, 3]$ of diagrams in Fig. 15.

smooth subintervals Fig. 21, but not in the chaotic regime where the extreme sensitivity of the calculation renders the individual orbits essentially uncomputable in the deterministic sense (Fig. 20), despite the fact that the trajectory energy errors are converging to zero (Fig. 23).

This example illustrates one of the most important reasons for using structure-preserving integrators. In the smooth regime, almost any integrator can achieve reasonable results on a fixed time interval with a sufficiently small timestep. This can be viewed as a direct consequence of the convergence of the method. On the other hand, *in the chaotic regime, nothing can be said regarding the global error of a trajectory*, and we are forced to rely on other properties of the integrator in question (such as preservation of physical properties of the dynamical system) to argue for the validity of our computation.

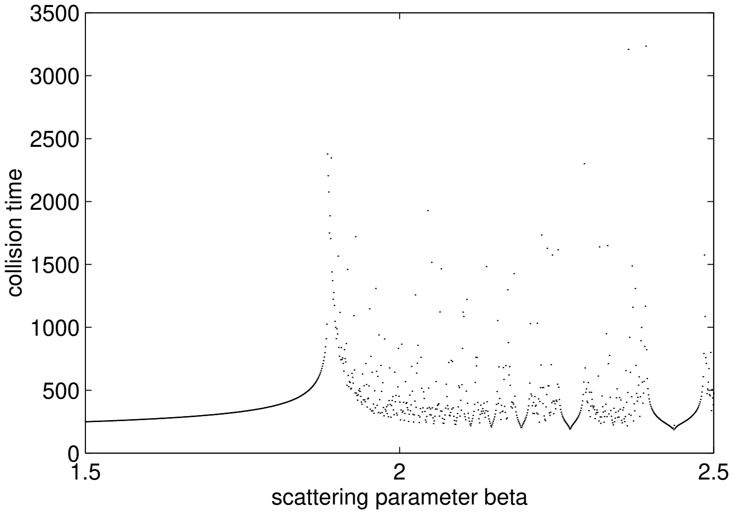

Figure 17: Collision times for $\beta \in [1.5, 2.5]$, $\Delta\tau = 0.01$.

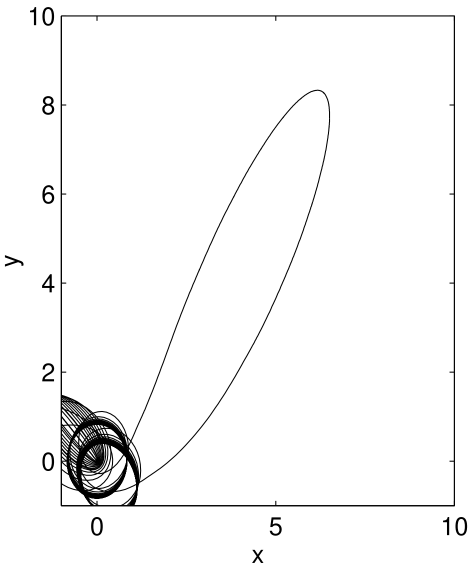

0.75truein (a)

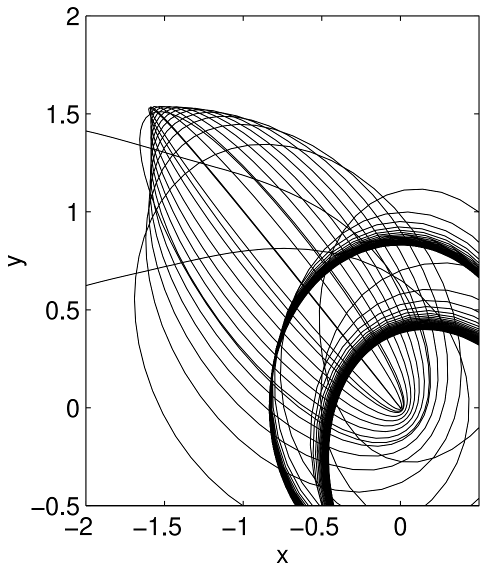

(b)

Figure 18: Close-ups of orbit for $\beta = 2.1$ for (a) a long bounded excursion, and (b) corresponding precessing elliptical orbits of the inner electron.

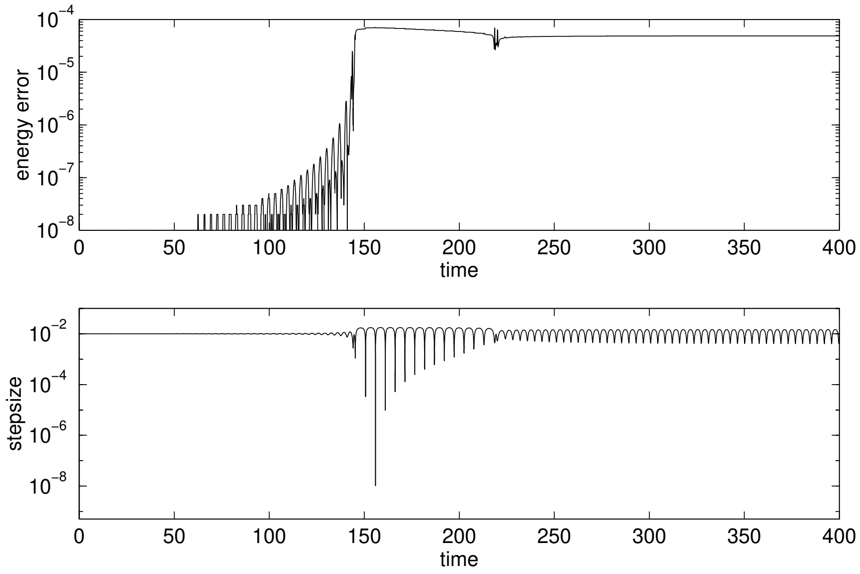

Figure 19: Energy error (upper graph) and stepsize variation (lower) for $\beta = 2.1$, $\Delta\tau = 0.01$.

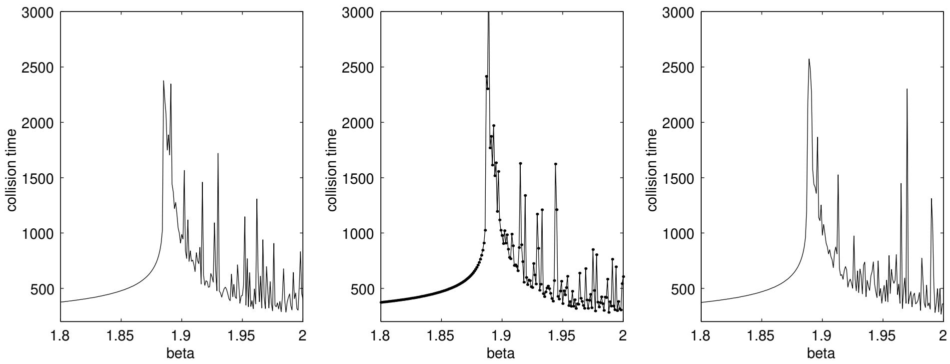

Figure 20: Collisions times converge only in the smooth regime (a) $\Delta\tau = 0.01$, (b) $\Delta\tau = 0.005$, (c) $\Delta\tau = 0.0025$

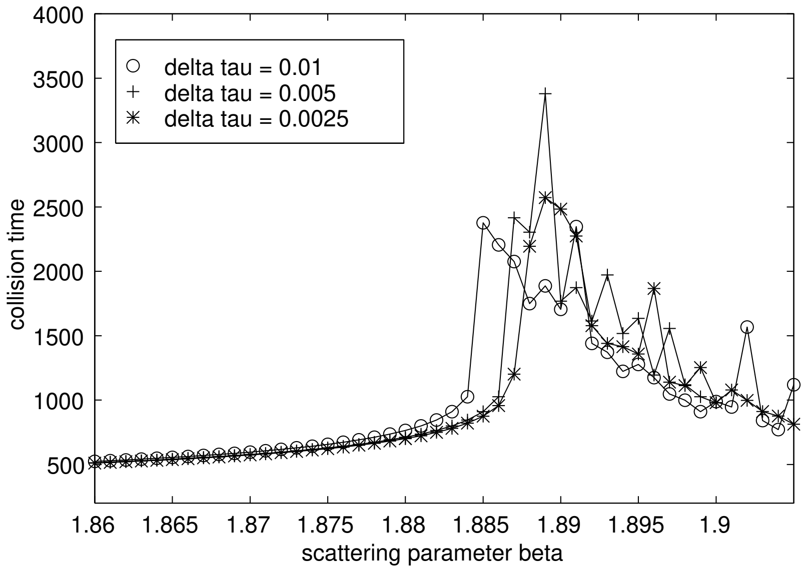

Figure 21: Superposition of graphs in Fig. 20.

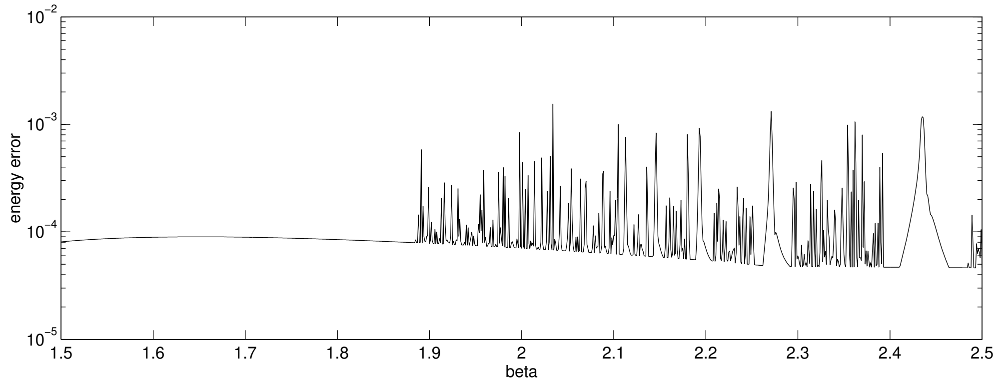

Figure 22: Energy errors as a function of the scattering parameter β for $\Delta\tau = 0.01$.

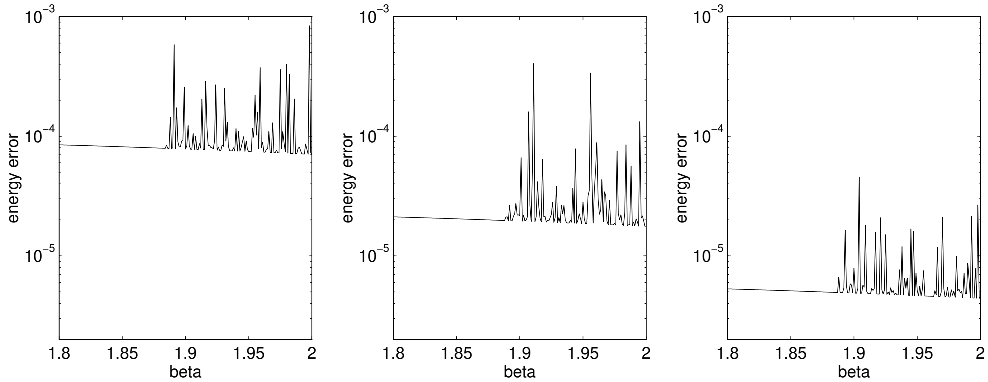

Figure 23: Energy errors by stepsize (a) $\Delta\tau = 0.01$, (b) $\Delta\tau = 0.005$, (c) $\Delta\tau = 0.0025$

8 Conclusion

A reversible adaptive regularizing scheme for perturbed Kepler problems and certain types of classical N-body problems has been presented. This method uses a special Sundman transformation, the Adaptive Verlet method, KS regularization, and a fast Kepler solver. The resulting algorithm performs well in the examples looked at. What has not been shown is how to use these methods in problems with three-body close approaches and which require specialized N-body techniques for their stable treatment. These issues will be examined in a forthcoming article.

Acknowledgement

For useful suggestions and discussions regarding regularization, the author thanks Sverre Aarseth (Cambridge Institute of Astronomy). For helpful discussions on nonlinear dynamics, the author thanks Robert MacKay (DAMTP/Nonlinear Centre). For suggestions and discussions regarding the applications, the author thanks Gregor Tanner (Hewlett-Packard BRIMS) and Colm Whelan and Jens Rasch (DAMTP/Atomic Theory Group). The author also warmly acknowledges the considerable moral support provided by Arieh Iserles (DAMTP) and the successful efforts of Mike Powell and David Crighton (DAMTP) to arrange financial support at unreasonably short notice.

References

[1] Aarseth, S.J., Direct methods for N-body simulation, in *Multiple Time Scales*, eds. J.U. Brackbill and B.I. Cohen, Academic Press, NY, 1985.

[2] E. Barth, B. Leimkuhler and S. Reich, A semi-explicit, variable stepsize, time-reversible integrator for constrained dynamics, preprint, 1996.

[3] G. Benettin and A. Giorgilli, On the Hamiltonian interpolation of near-to-the-identity symplectic mappings with application to symplectic integration algorithms, J. Statist. Phys. **74**, 1117, 1994.

[4] F. Benvenuto, G. Casati, and D. Shepelyansky, Dynamical localization: hydrogen atoms in magnetic and electrical fields, Phys. Rev. **A 55**, 1732, 1997.

[5] R. Bulirsch and J. Stoer, *Introduction to Numerical Analysis*, Springer, 1980.

[6] M.P. Calvo and J.M. Sanz-Serna, The development of variable stepsize symplectic integrators with application to the two-body problem, SIAM J. Sci. Comp. **14**, 936, 1993.

[7] G. Ezra, K. Richter, G. Tanner, and D. Wintgen, J. Phys. **B 24**, L413, 1991

[8] J. Frank, W. Huang and B. Leimkuhler, Geometric Integrators for Classical Spin Systems, J. Comput. Phys., to appear, 1997.

[9] Y. Funato, P. Hut, S. McMillan, and J. Makino, Time-Symmetrization of Kustaanheimo-Stiefel Regularization, Astrophysics J. **112**, 1697, 1996.

[10] Z. Ge and J. Marsden, Lie-Poisson Hamilton-Jacobi theory and Lie-Poisson integrators, Phys. Lett. **A 133**, 134, 1988.

[11] O. Gonzales and A.M. Stuart, Remarks on the qualitative properties of the modified equations, preprint, SCCM program, Stanford, CA, 1996.

[12] Y. Gu and J.-M. Yuan, Chaotic scattering of electrons with He^+, Phys. Rev. **A 47**, R2442, 1993.

[13] M. Gutzwiller, *Chaos in Classical and Quantum Mechanics*, Springer, NY, 1990.

[14] E. Hairer, Variable timestep integration with symplectic methods, preprint, Dept. of Mathematics, Geneva, 1996.

[15] E. Hairer, Backward analysis of numerical integrators and symplectic methods, Annals of Numerical Mathematics **1**, 107, 1994.

[16] D.C. Heggie, Cel. Mech. **10**, 185, 1974.

[17] D.C. Heggie, The N-body problem in stellar dynamics, in *Long-Term Dynamical Behavior of Natural and Artificial N-Body Systems*, Ed. A.E. Roy, Kluwer, Dordrecht, 1988.

[18] W. Huang and B. Leimkuhler, The Adaptive Verlet Method, SIAM J. Sci. Comp. **18**, 239, 1997.

[19] P. Hut, J. Makino, S. McMillan, Building a better leapfrog, The Astrophysical Journal **443**: L93-L96, 1995.

[20] P. Hut, Funato, Y., Kokubo, E., J. Makino, S. McMillan, Time symmetrization meta-algorithms, in *Computational Astrophysics,* Proc. of the 12th 'Kingston meeting' on Theoretical Astrophysics, Eds. D.A. Clarke and M.J. West, ASP Conf. Series, to appear.

[21] P. Kustaanheimo and E. Stiefel, Perturbation theory of Kepler motion based on spinor regularization, J. Reine Angew. Math., **218**, 204, 1965.

[22] Lecar, M., Comparison of eleven numerical integrations of the same gravitational 25-body problem, Bull. Astron. **3**, 91, 1968.

[23] E. Lee, A. Brunello, and D. Farrelly, Coherent states in a Rydberg atom: classical mechanics, Phys. Rev. **A 55**, 2203, 1997.

[24] R.S. MacKay, Some aspects of the dynamics and numerics of Hamiltonian systems, in Proc. of the IMA Conf. on the Dynamics of Numerics and the Numerics of Dynamics, Eds. J. Broomhead and A. Iserles, Cambridge University Press, Cambridge, UK, 1990.

[25] J. Main and G. Wunner, Hydrogen atom in a magnetic field: ghost orbits, catastrophes, and uniform semiclassical approximation, J. Phys. **A 55**, 1743, 1997.

[26] J. Marsden, Lectures on mechanics, Cambridge U. Press, Cambridge, 1992.

[27] R. McLachlan, G.R.W. Quispel, and G.S. Turner, Numerical integrators that preserve symmetries and reversing symmetries, preprint, 1996.

[28] D. Noid, S. Gray, and S. Rice, J. Chem. Phys. **85**, 2649, 1986.

[29] S. Reich, Backward error analysis for numerical integrators, preprint, 1996.

[30] K. Richter, and Wintgen, W., J. Phys. **B 23**, L197 1990.

[31] K. Richter, G. Tanner, and W. Wintgen, J. Phys. **A 48**, 4182 1993.

[32] R.D. Ruth, A canonical integration technique, IEEE Trans. Nucl. Sci. **30**, 2669, 1983.

[33] K. Rzazewski, M. Lewenstein, and P. Salieres, Multielectron stabilization of atoms in a laser field: classical perspective, Phys. Rev. **A 49**, 1196, 1994.

[34] J.M. Sanz-Serna and M.P. Calvo, *Numerical Hamiltonian Problems*, Chapman and Hall, 1994.

[35] C.L. Siegel, and J.K. Moser, *Lectures on Celestial Mechanics*, Springer, Berlin, 1971.

[36] J. Steckel and C. Jaffe, The Bifurcations of the Langmuir Orbit in the Two-Electron Atom, Hamiltonian Systems with three or more degrees of freedom, NATO ASI Series, Kluwer Academic Publishers, submitted.

[37] D. Stoffer, Variable steps for reversible integration methods, Computing **55**,1, 1995.

[38] Q. Wang and A. Sterace, Classical interpretation of the quantum description of H^- photodetachment in parallel E and B fields, Phys. Rev. A **55**, 815, 1997.

[39] R.F. Warming and B.J. Hyett, The modified equations approach to the stability and accuracy of finite difference methods, *J. Comput. Phys.* **14**, 159, 1974.

Appendix A. Elementary numerical methods.

The following schemes are described for an initial value problem of the form $\dot{z} = f(z)$, $z(0) = z_0$. $z_n \approx z(t_n)$, $t_n = n\Delta t$, $n = 0, 1, \ldots$.

Euler's Method

$$z_{n+1} := z_n + \Delta t f(z_n)$$

Heun's Method (second order)

$$\bar{z} := z_n + \Delta t f(z_n); \qquad z_{n+1} := z_n + \frac{1}{2}\Delta t(f(z_n) + f(\bar{z}))$$

Explicit Runge-Kutta (fourth order)

$$Z_1 := z_n + \frac{1}{2}\Delta t f(z_n); \qquad Z_2 := z_n + \frac{1}{2}\Delta t f(Z_1); \qquad Z_3 := z_n + \Delta t f(Z_2);$$

$$z_{n+1} := z_n + \Delta t(\frac{1}{6}f(z_n) + \frac{1}{3}f(Z_1) + \frac{1}{3}f(Z_2) + \frac{1}{6}f(Z_3))$$

Implicit Midpoint Method (second order)

$$z_{n+1} := z_n + \Delta t f(\bar{z}); \qquad \bar{z} = \frac{z_n + z_{n+1}}{2}$$

The following schemes are described for an initial value problem of the form $\dot{q} = f(p); \dot{p} = g(q)$, $q(0) = q_0$, $p(0) = p_0$. $(q_n, p_n) \approx (q(t_n), p(t_n))$, $t_n = n\Delta t$, $n = 0, 1, \ldots$.

Symplectic Euler Method (first order)

$$\begin{aligned} q_{n+1} &:= q_n + \Delta t f(p_{n+1}) \\ p_{n+1} &:= p_n + \Delta t g(q_n) \end{aligned}$$

Leapfrog (Verlet) Method (second order)

$$\begin{aligned} q_{n+1} &:= q_n + \Delta t f(p_{n+1/2}) \\ p_{n+1/2} &:= p_n + \frac{1}{2}\Delta t g(q_n) \\ p_{n+1} &:= p_n + \frac{1}{2}\Delta t g(q_{n+1}) \end{aligned}$$

Ruth Method (third order)

$$\begin{aligned} Q_1 &:= q_n + \frac{7}{24}\Delta t f(P_1)) \\ P_1 &:= p_n + \frac{2}{3}\Delta t g(q_n) \\ Q_2 &:= Q_1 + \frac{3}{4}\Delta t f(P_2)) \\ P_2 &:= P_1 - \frac{2}{3}\Delta t g(Q_1) \\ q_{n+1} &:= Q_2 - \frac{1}{24}\Delta t f(p_{n+1}) \\ p_{n+1} &:= P_2 + \Delta t g(Q_2) \end{aligned}$$

Appendix B. RAR Methods.

In this appendix, for convenience, we give pseuodcode algorithms for the RAR methods for treating perturbed Kepler problems and atomic dynamics.

B.1 Definitions.

Kustaanheimo-Stiefel transformation.

$$(Q, P) = \mathrm{KS}(q, p),$$

obtained by solving (4.11), (4.12) (with arbitrary choice of the guage freedom) for Q, P, (see [21] for formulae) and corresponding inverse map:

$$(q, p) = \mathrm{KS}^{-1}(Q, P)$$

defined directly by equation (4.11),(4.12).

KS Time Transformation.

Compute $\Delta s = \mu(\Delta t)$ by solving (4.20) (alternatively (4.16) for very close approaches) using a Newton iteration.

KS Solve.

Compute $(\hat{Q}, \hat{P}) = \Phi_{\Delta s}(Q, P)$, the solution of the linear system in the transformed variables using (4.17)-(4.18) with timestep Δs. This requires the solution of 2×2 linear systems. Alternatively solve (4.14)-(4.15) for a time interval Δs.

Outer Sundman Transformation.

Define control function g by

$$g(q) = (1 + |q|^{-a})^{-1}$$

B.2 Perturbed Kepler Problem Timestep Algorithm

Given: $\Delta\tau$ fixed, q_0, p_0, initial (previous) timestep Δt_0, this algorithm applies the RAR method to solve

$$H = \frac{1}{2}|p|^2 - \frac{1}{|q|} + \hat{H}(p, q).$$

for one fictive timestep $\Delta\tau$, yielding (q_1, p_1).

1. Compute the new timestep by

$$\Delta t_1 := \left(\frac{2}{g(q_0)} - \frac{\Delta\tau}{\Delta t_0}\right)^{-1} \Delta\tau$$

2. Solve the perturbation Hamiltonian $\hat{H}$ for a timestep of size $\frac{1}{2}\Delta t_1$, using either the exact solution (if easily computed) or an approximation. Store result in $(\hat{q}_0, \hat{p}_0)$.

3. $(Q_0, P_0) := \mathrm{KS}(\hat{q}_0, \hat{p}_0)$.

4. Compute KS timestep $\Delta s := \mu(Q_0, P_0, \Delta t_1)$.

5. Compute KS solution $(Q_1, P_1) := \Phi_{\Delta s}(Q_0, P_0)$.

6. $(\hat{q}_1, \hat{p}_1) := \mathrm{KS}^{-1}(Q_1, P_1)$.

7. Repeat step (2) from $(\hat{q}_1, \hat{p}_1)$. Result is (q_1, p_1).

Note: The fictive timestep computation (step 4.) can be accellerated by use of a good predictor for the new Δs. We had good results by storing Δs_n at the nth timestep and then using as predictor

$$\Delta s^{\mathrm{P}}_{n+1} := \frac{\Delta t_{n+1}}{\Delta t_n} \Delta s_n,$$

in the Newton iteration defining μ.

B.3 Adjustments for Atomic Systems

For the atomic problem, the only modifications to the algorithm of §B.2 are as follows.

(i) We replace the time transformation by

$$g(q) = (1 + r_{\mathrm{en}}{-a} + r_{\mathrm{ee}}^{-b})^{-1},$$

where $r_{\mathrm{en}} = \min_i |q_i|$, and $r_{\mathrm{ee}} = \min_{i \neq j} |q_i - q_j|$.

(ii) The perturbation Hamiltonian at steps 2. and 7. is replaced by the electron-electron interaction potential.

(iii) The fast KS solve in steps 3.-6. is performed for each of the N electrons in the system.

(iv) Fictive timestep values should be stored for each electron, in order to predict Δs for each electron to improve convergence of the timestep iteration (step 4.).

Appendix C. Treatment of Electrical and Magnetic Fields

In this appendix, we show how applied electrical and magnetic fields can be incorporated into the reversible adaptive regularization method, an important aspect since Rydberg atom systems typically involve such fields [25, 4]. Although we primarily describe the case of static fields, the technique described could be extended to handle time–or space–dependencies.

Through splitting, we first reduce a multiple electron atom to individual electron-nucleus interactions, i.e. the hydrogenic case. For hydrogen, the Hamiltonian in constant electrical and magnetic fields is

$$H = \frac{1}{2}|p - \frac{1}{2}\hat{B}q|^2 - \frac{1}{|q|} + E \cdot q,$$

with $E \in \mathbb{R}^3$, $B = (b_1, b_2, b_3)^T \in \mathbb{R}^3$ and

$$\hat{B} = \mathrm{skew}(B) = \begin{bmatrix} 0 & b_3 & -b_2 \\ -b_3 & 0 & b_1 \\ b_2 & -b_1 & 0 \end{bmatrix}.$$

For the case of parallel static fields, it is convenient to represent the problem in semi-parabolic coordinates, as in [38]. To do this, assume that $E = (0, 0, \sigma)$ and $B = (0, 0, \gamma)$ are fixed. The key observation is that the z-component of angular momentum remains an invariant (the Hamiltonian posesses rotational symmetry about the z-axis). We introduce polar coordinates,

$$H = \frac{1}{2}(p_r^2 + p_z^2) + \frac{l^2}{r^2} + \frac{\gamma l}{r} + \frac{1}{8}\gamma^2 r^2 - \frac{1}{r^2 + z^2} + \sigma z$$

where l is the angular momentum, and follow this with the change of variables $r = u^2 - v^2$, $z = 2uv$. After a time transformation $g = u^2 + v^2$, we find

$$\begin{aligned} \tilde{H} \;=\; & \frac{1}{8}(p_u^2 + p_v^2) + \frac{l^2(u^2 + v^2)}{(u^2 - v^2)^2} + \frac{\gamma l}{u^2 - v^2} + \frac{1}{8}\gamma^2(u^2 - v^2)^2(u^2 + v^2) - 1 \\ & + 2\sigma uv(u^2 + v^2) - H_0(u^2 + v^2) \end{aligned}$$

This approach, when combined with a reversible-adaptive integrator such as Adaptive Verlet can lead to rather good behavior [38], esp. when $l = 0$ and the singular terms vanish. For arbitrary field alignments, or for moving fields, the angular momentum is no longer a conserved quantity, and a more general approach is needed.

8.1 A splitting method for fields

For the general case we propose to introduce the splitting $H = H^{\mathrm{Kep}} + H^{\mathrm{B}} + H^{\mathrm{E}}$, with

$$H^{\mathrm{Kep}} = \frac{|p|^2}{2} - \frac{1}{|q|}, \qquad H^{\mathrm{B}} = -\frac{1}{2}(p^T\hat{B}q - \frac{1}{8}q^T\hat{B}^2 q), \qquad H^{\mathrm{E}} = E \cdot q$$

The first part can be integrated using the KS-transformation (or the fast Kepler solver). In the case of constant fields, the second and third parts are integrable: under H^{B}, q can be evolved from q^{old} to q^{new} via a rotation about B,

$$q^{\mathrm{new}} = \exp(-\frac{1}{2}\Delta t\hat{B})q^{\mathrm{old}}$$

which is easily and efficiently computed using Rodrigue's formula:

$$\exp(\alpha\hat{B}) = \cos(\alpha|B|)I + \frac{\sin(\alpha|B|)}{|B|}\hat{B} + \frac{(1-\cos(\alpha|B|)}{|B|^2}BB^T.$$

Then the corresponding update to p can be obtained by solving the resulting 3×3 linear system

$$\dot{p} = -\frac{1}{2}\hat{B}p - \frac{1}{4}\hat{B}^2 q.$$

In a timestep, this yields

$$\begin{aligned} p^{\mathrm{new}} &= \exp(-\frac{1}{2}\Delta t\hat{B})p^{\mathrm{old}} - \frac{1}{4}\int_0^{\Delta t}\exp(-\frac{1}{2}(\Delta t-\tau)\hat{B})\hat{B}^2\exp(-\frac{1}{2}\tau\hat{B})q^{\mathrm{old}}ds, \\ &= \exp(-\frac{1}{2}\Delta t\hat{B})(p^{\mathrm{old}} - \frac{1}{4}\Delta t\hat{B}^2 q^{\mathrm{old}}), \end{aligned}$$

where we have used the fact that the exponential of $\hat{B}$ commutes with $\hat{B}$. Thus just a single additional rotation about B is needed. Finally, the electrical field term is p-independent and therefore also easily integrated.

This method could be adapted to the case of time–or position-dependent fields by invoking appropriate symplectic approximations for the field perturbations.

We use a symmetric splitting, the Sundman transformation of the last section, and the Adaptive Verlet method to combine the various parts into a usable method. The justification for using such a splitting is that during the critical close approaches to the nucleus, we have,

$$\begin{aligned} |p| &\sim |p - \frac{1}{2}\hat{B}q|, \\ &\sim \sqrt{2\left(H_0 + \frac{1}{|q|}\right)}, \\ &\sim \sqrt{2}|q|^{-1/2}, \end{aligned}$$

where we have used the conservation of energy. Thus the force contribution from the magnetic field term is on the order of the fourth root of the Coulombic force in this regime. Other perturbations are typically even smaller.

In the absence of ionizing trajectories, the presence of fields doesn't require any modification of the time transformation.[3]

[3] For ionizing orbits in electrical and magnetic fields, some adjustment of the time transformation is necessary in order to accurately follow escaping trajectories. We obtained good results by simply modifying the step control function g to

$$g(q) = \frac{1}{r_{\mathrm{en}}^{-a} + r_{\mathrm{ee}}^{-b} + r_{\max} + 1},$$

where $r_{\max}$ represents the largest radial component of any of the electron components.

8.2 Numerical experiment: hydrogen in parallel fields

We apply this method to treat hydrogen in parallel fields. As noted at the beginning of the section, this problem can be solved using semiparabolic coordinates; it is interesting that the general reversible adaptive regularization method, which does not specifically make use of the known angular momentum, also performs well.

We fixed $E = (0, 0, 1)$, set $B = (0, 0, \gamma)$, and varied γ, plotting electron positions for $t \in [0, 500]$ using fictive stepsize $ds = 0.01$. For small values of γ, the electron motion appears to be quasiperiodic (Fig. 24, top, $\gamma = 0.6$). For larger values, the orbit becomes ergodic and fills a region of space (Fig. 24, center, $\gamma = 4$). (The darkening in the center is not a reflection of the physical density of trajectories there; it is an artifact of the larger numbers of timesteps placed near the origin due to the step control.) Near $\gamma = 6$ a two-dimensional structure begins to emerge, and is refined at about $\gamma = 8$ (Fig. 24, bottom). The graphs are suggestive of tori motion, indicating the presence of a nearby periodic orbit. At $\gamma = 7.796$, and $E = (0, 0, 1.012625)$ we indeed find such a periodic orbit (Fig. 25), making approaches within $|q| = 10^{-7}$ of the nucleus. Periodic orbits very similar to this one are mentioned in [13], and are important to the current understanding of the semiclassical theory. Despite the close approaches, the stepsize is smoothly controlled during the collision, and the energy is strikingly well-behaved (Fig. 26).

Observe in particular that during close approach, the orbit takes the appearance of a pure Kepler orbit (with the associated symmetry properties).

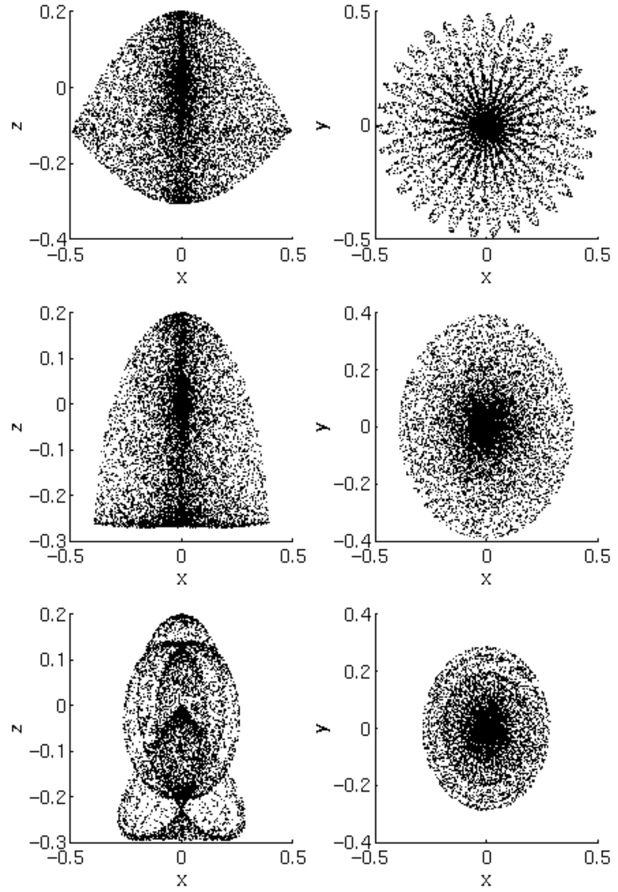

Figure 24: Side and top views of orbits of hydrogen in parallel fields: top $\gamma = 0.6$, center $\gamma = 4$, and bottom, $\gamma = 8$.

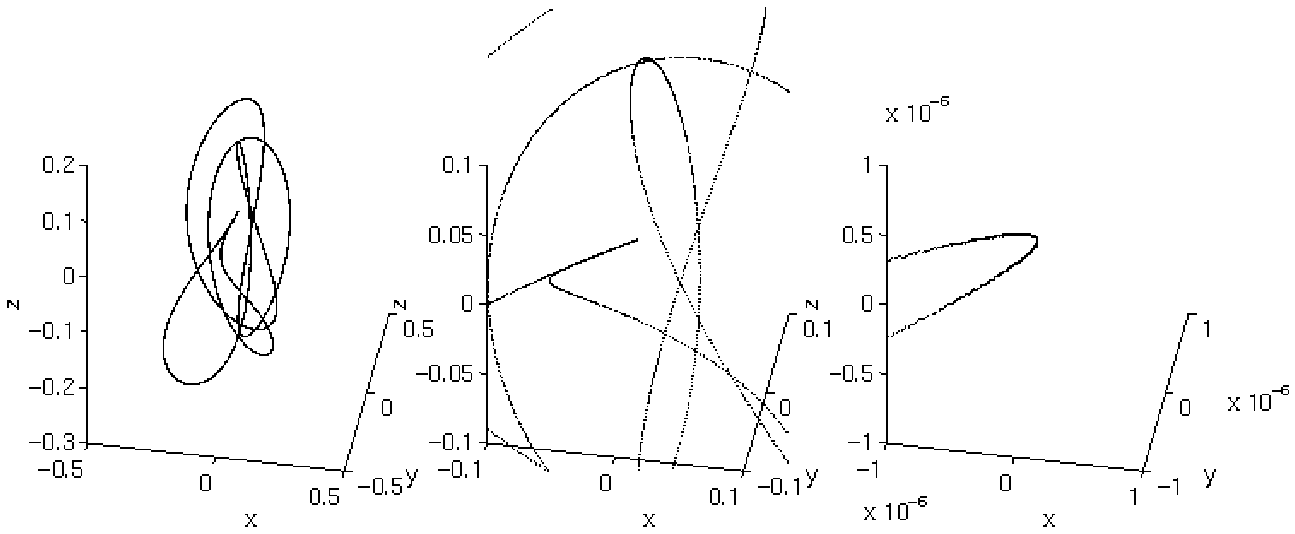

Figure 25: Periodic orbit at At $\gamma = 7.796$, and $E = (0, 0, 1.012625)$, with close-ups of the origin.

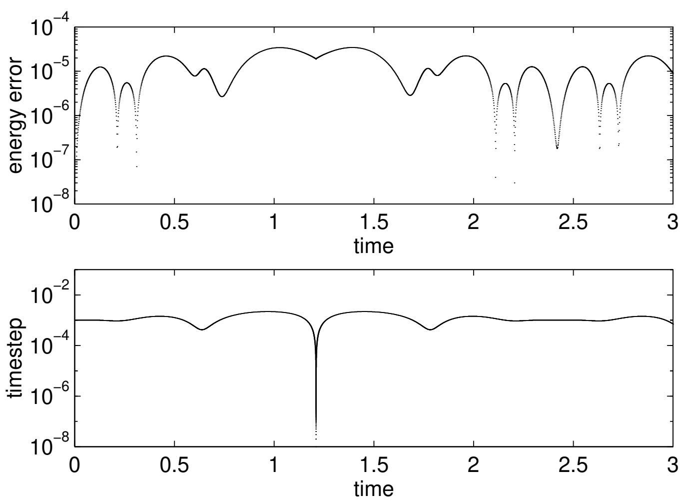

Figure 26: Energy variation and timestep variation over approximately one period of the motion. Despite the requirement for small steps in the vicinity of the origin, the energy is very well controlled. Longer simulations revealed no noticeable drift in energy.